

Correcting biased noise using Gottesman-Kitaev-Preskill repetition code with noisy ancilla

Zhifei Li  and Daiqin Su*

MOE Key Laboratory of Fundamental Physical Quantities Measurement, Hubei Key Laboratory of Gravitation and Quantum Physics, PGMF, Institute for Quantum Science and Engineering, School of Physics, Huazhong University of Science and Technology, Wuhan 430074, China

 (Received 22 August 2023; accepted 19 April 2024; published 13 May 2024)

Concatenation of a bosonic code with a qubit code is one of the promising ways to achieve fault-tolerant quantum computation. As one of the most important bosonic codes, the Gottesman-Kitaev-Preskill (GKP) code is proposed to correct small displacement errors in phase space. If the noise in phase space is biased, the square-lattice GKP code can be concatenated with the repetition code that promises a high fault-tolerant threshold to suppress the logical error. In this work, we study the performance of GKP repetition codes with finite-energy ancillary GKP qubits in correcting biased noise. We find that there exists a critical value of noise variance for the ancillary GKP qubit such that the logical Pauli error rate decreases when increasing the code size. Furthermore, one round of GKP error correction has to be performed before concatenating with the repetition code. Our study paves the way for practical implementation of error correction by concatenating the GKP code with low-level qubit codes.

DOI: [10.1103/PhysRevA.109.052420](https://doi.org/10.1103/PhysRevA.109.052420)

I. INTRODUCTION

Noise is the main hindrance to achieve large-scale fault-tolerant quantum computation. A quantum error correcting code is introduced to correct errors by using redundancy in the Hilbert space [1–3]. Bosonic codes protect finite-dimensional logical space by encoding it in an infinite-dimensional bosonic quantum system [4,5], e.g., a simple harmonic oscillator. Compared to the standard qubit codes that encode a single logical qubit using many physical qubits, the bosonic code is more hardware efficient and is subject to a smaller number of noisy channels [6,7]. Currently well-established bosonic codes include the Gottesman-Kitaev-Preskill (GKP) code [8,9], cat code [10,11], binomial code [6,12–14], and rotation-symmetric code [15,16]. The GKP code is one of the most promising bosonic codes, which corrects small displacement errors in phase space and also photon loss [6,17]. Although the GKP code has been proposed for two decades [8], it was prepared only recently in ion-trapped [18,19] and superconducting [20] platforms, and was used to extend the coherence time of the logical qubit through error correction [21]. The GKP code has promising advantages in optical quantum information processing [22], however, optical GKP states have not been experimentally generated due to the stringent requirement for strong nonlinearity, though various preparation schemes have been proposed [23–27].

To achieve fault tolerance, the common strategy is to concatenate the GKP code with qubit codes to further suppress the logical error. Examples include concatenation with surface or toric codes [28–33], color code [34–36], and so on. Concatenation with qubit codes with a high threshold enables a low squeezing threshold for the GKP states around

10 dB [28], which is within the reach of near-term technologies. A variant of the original surface code, known as the $XZZX$ surface code [37], has recently been shown to have a higher threshold for biased noise. It is expected that concatenation of GKP code with $XZZX$ surface code would enable a lower squeezing threshold if the displacement error is biased [38]. This can happen in two cases, either the noise is biased and a square-lattice (isotropic) GKP code is used, or the noise is isotropic and a biased GKP code is used. However, syndrome measurement and decoding are still complicated for the $XZZX$ surface code [39], which therefore consume more physical and computational resources. A relatively easier scheme to suppress biased noise is to concatenate the GKP code with the repetition code [40], which requires easier syndrome measurement and decoding and has a higher threshold. In Ref. [40], the error threshold was estimated for biased GKP repetition code with isotropic noise, which outperformed the biased planar surface code [30]. However, both the data and ancillary GKP qubits were assumed to be ideal, namely, with infinite energy. The error threshold as derived in Ref. [40], therefore, only provided an upper bound, and the requirement was more stringent when the imperfections from the ancillary GKP qubits were taken into account.

In this work, we study the concatenation of a square-lattice GKP code with a repetition code to correct biased displacement errors, where both the data and ancillary GKP qubits have finite energy. The error correction procedure consists of four steps: encoding; one round of GKP error correction; syndrome measurement on the repetition code; and recovery operation according to the measurement outcomes. We find that the GKP error correction with finite-energy ancillary GKP qubits, in general, increases the logical Pauli error rate of the GKP code as compared to that with ideal ancillary GKP qubits. However, this does not ruin the error correction procedure but is actually necessary to exploit the power of

*sudaiqin@hust.edu.cn

code concatenation. We also find that the logical Pauli error rate decreases when increasing the size of the repetition code if the noise variance of the ancillary GKP qubits is sufficiently small, while the logical Pauli error rate increases when increasing the size of the repetition code if the noise variance is too large. This implies that there exists a critical value of noise variance for the ancillary GKP qubits below which the code concatenation shows advantages. Our results set an upper bound for the noise variance of the ancillary GKP qubits such that the concatenation with repetition code is useful.

The paper is organized as follows. In Sec. II we briefly review the ideal (infinite-energy) and finite-energy GKP states and introduce the biased noise model. We then discuss the GKP error correction with finite-energy ancillary GKP qubits to correct small displacement errors in position space in Sec. III. In Sec. IV we concatenate the GKP code with the repetition code to reduce the logical Pauli error rate in position space and estimate the critical value of noise variance for the ancillary GKP qubit. Then in Sec. V we use GKP repetition code to correct biased noise to reduce the overall logical error rate, taking into account the effects of displacement errors in momentum space. We finally conclude in Sec. VI.

II. GKP STATES AND NOISE MODEL

Ideal GKP states are common eigenstates of two commuting operators, $\hat{S}_q = \hat{X}(2\sqrt{\pi})$ and $\hat{S}_p = \hat{Z}(2\sqrt{\pi})$ [8], where $\hat{X}(u) = e^{-iu\hat{p}}$ and $\hat{Z}(v) = e^{iv\hat{q}}$ are displacements along position and momentum, respectively. They form a two-dimensional code subspace of an infinite-dimensional Hilbert space of a bosonic system, the computational bases of which can be chosen as

$$|j\rangle = \sum_{n=-\infty}^{+\infty} |(2n+j)\sqrt{\pi}\rangle_q, \quad (1)$$

where $j = 0, 1$, and the subscript “ q ” indicates a position eigenstate.

Ideal GKP states have infinite energy and cannot be prepared in practice. A finite-energy GKP state can be obtained by applying an envelope operator to an ideal GKP state [41] or through coherently superposing randomly displaced ideal GKP states [8,9], namely,

$$|\tilde{\psi}\rangle = N \int dudv \eta(u, v) \hat{D}(u, v) |\bar{\xi}\rangle, \quad (2)$$

where $|\bar{\xi}\rangle$ is an ideal GKP state, $\hat{D}(u, v) = e^{-iu\hat{p}+iv\hat{q}}$ is a displacement operator, N is a normalization factor, and $\eta(u, v)$ is the probability amplitude that is chosen as a bivariate Gaussian distribution

$$\eta(u, v) = \frac{1}{\sqrt{\pi\kappa\Delta}} \exp\left[-\frac{1}{2}\left(\frac{u^2}{\Delta^2} + \frac{v^2}{\kappa^2}\right)\right], \quad (3)$$

with Δ and κ the standard deviations. It can be shown that the finite-energy GKP state defined in Eq. (2) is normalizable (see Appendix A for details) and therefore contains a finite amount of energy.

The noise model that we consider is an anisotropic Gaussian displacement channel (GDC), namely, the noise in one quadrature and its conjugate quadrature are generally not the

same. Since we use the square-lattice GKP code, a biased logical error will be induced due to the anisotropic GDC, which is further corrected by concatenating with the repetition code. This is mathematically equivalent to the scheme where an isotropic GDC is considered while the GKP code is biased [40]. We consider the first because it is experimentally easier to generate the square-lattice GKP code states with biased noise.

The density matrix transforms as

$$\hat{\rho} \rightarrow \mathcal{N}_f(\hat{\rho}) = \int dudv f(u, v) \hat{D}(u, v) \hat{\rho} \hat{D}^\dagger(u, v), \quad (4)$$

when the bosonic system is acted upon by a GDC, where $f(u, v)$ is a bivariate Gaussian distribution. According to the definition (4) the input state is imposed on a random displacement $\hat{D}(u, v)$ each time and the output state is an incoherent mixture of all possible displacements. This results in a blurred output Wigner function.

The GDC is different from the coherent superposition of random displacements that involved in defining finite-energy GKP states in Eq. (2), in particular, a finite-energy GKP state cannot be generated by simply passing an ideal GKP state through a GDC (see Appendix A for details). However, these two sets of states have exactly the same noise property if $f(u, v) = |\eta(u, v)|^2$, except that the finite-energy GKP state has an envelope. Therefore, we can treat the noise in the finite-energy GKP state in the same way as we treat the noise from the GDC when the envelope is irrelevant.

Since the displacement errors in position and momentum spaces are independent, the error distribution $f(u, v) = f_q(u)f_p(v)$, with

$$f_q(u) = \frac{1}{\sqrt{\pi}\Delta} e^{-\frac{u^2}{\Delta^2}}, \quad f_p(v) = \frac{1}{\sqrt{\pi}\kappa} e^{-\frac{v^2}{\kappa^2}}. \quad (5)$$

For unbiased noise, we have $\Delta = \kappa$. In this paper, we consider biased noise where the noise in one quadrature is suppressed while that in the conjugate quadrature is amplified. The error distribution of biased noise can be parameterized as

$$f_q(u) = \frac{1}{\sqrt{\pi}r\Delta} e^{-\frac{u^2}{(r\Delta)^2}}, \quad f_p(v) = \frac{r}{\sqrt{\pi}\Delta} e^{-\frac{v^2}{(\Delta/r)^2}}, \quad (6)$$

where r is a real positive number and represents the bias level. By choosing $r > 1$, the noise in momentum space is suppressed while that in position space is amplified. We then concatenate the GKP code with the repetition code to suppress the logical Pauli error induced by the large displacement error in position space. The Wigner function of the GKP code with unbiased and biased noise is shown in Fig. 1.

III. GKP ERROR CORRECTION WITH FINITE-ENERGY ANCILLARY QUBITS

In this section, we discuss the correction of displacement error in position space using the GKP code with ideal and finite-energy ancillary GKP qubits.

A. GKP error correction with ideal ancilla

The quantum error correction circuit using the SUM gate is shown in Fig. 2. An ancillary qubit couples with the data qubit

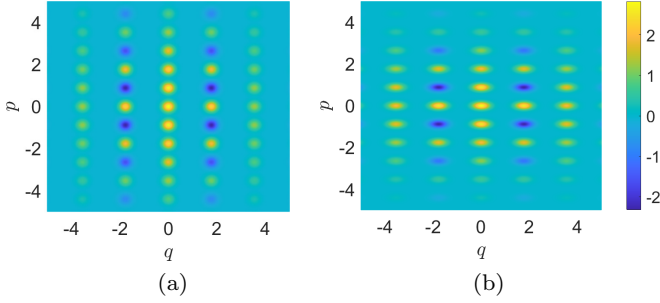


FIG. 1. Wigner function for finite-energy GKP states. (a) Wigner function of GKP state with unbiased noise, where $\Delta = 0.25$, $r = 1$. (b) Wigner function of GKP state with biased noise, where $\Delta = 0.25$, $r = \sqrt{2}$. The noise of momentum quadrature is suppressed, while the noise of position quadrature is amplified.

via the SUM gate, then its position quadrature is measured and the measurement outcome is fed forward to the data qubit [8]. Suppose the data qubit is prepared in a finite-energy GKP state $|\tilde{\psi}\rangle$ with $\eta(u, v)$ given by Eq. (3). Now we only consider correcting the displacement in position space and rewrite $|\tilde{\psi}\rangle$ as

$$|\tilde{\psi}\rangle = \int dv \eta(v) e^{iv\hat{q}} \int du \eta(u) e^{-iu v/2} |\psi(u)\rangle, \quad (7)$$

where $|\psi(u)\rangle$ is an ideal GKP state with position shifted by u ,

$$|\psi(u)\rangle = \alpha \sum_s |2s\sqrt{\pi} + u\rangle_{q_1} + \beta \sum_s |(2s+1)\sqrt{\pi} + u\rangle_{q_1}.$$

The ancillary qubit is assumed to be in the ideal GKP $|\bar{\dagger}\rangle$ state

$$|\bar{\dagger}\rangle = \sum_k |k\sqrt{\pi}\rangle_{q_2}. \quad (8)$$

The SUM gate is $e^{-i\hat{q}_1 \hat{p}_2}$, which preserves the position of the data GKP qubit while adds it to the position of the ancillary GKP qubit. The state after the SUM gate is therefore given by

$$\begin{aligned} & \int dv \eta(v) e^{iv\hat{q}} \int du \eta(u) e^{-iu v/2} \\ & \times \left[\alpha \sum_{s,k} |2s\sqrt{\pi} + u\rangle_{q_1} |(2s+k)\sqrt{\pi} + u\rangle_{q_2} \right. \\ & \left. + \beta \sum_{s,k} |(2s+1)\sqrt{\pi} + u\rangle_{q_1} |(2s+k+1)\sqrt{\pi} + u\rangle_{q_2} \right] \\ & = \int dv \eta(v) e^{iv\hat{q}} \int du \eta(u) e^{-iu v/2} \\ & \times |\psi(u)\rangle \left(\sum_k |k\sqrt{\pi} + u\rangle_{q_2} \right). \quad (9) \end{aligned}$$

The homodyne measurement of the ancillary qubit gives a fixed value for \hat{q}_2 ,

$$q_2 = k\sqrt{\pi} + u, \quad (10)$$

with k an integer. This implies that the superposition of different displacements is destroyed and the state in Eq. (9)

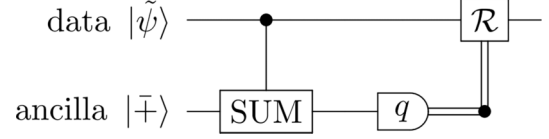


FIG. 2. Quantum circuit for GKP error correction. The ancillary GKP qubit is prepared in state $|\bar{\dagger}\rangle$ and then couples with the data GKP qubit via a SUM gate. The position shift of the data qubit propagates to the ancillary qubit and is detected by measuring the position of the ancillary qubit. Recovery is finally executed according to the measurement outcome.

collapses to a component with a fixed u . However, the superposition between GKP states $|\bar{0}\rangle$ and $|\bar{1}\rangle$ (shifted by u) is preserved since they cannot be distinguished by the measurement outcome.

Since we consider small displacement errors, so with a high probability q_2 deviates from $k\sqrt{\pi}$ in a small amount. Therefore, we infer the true value of u by subtracting from q_2 the nearest $k\sqrt{\pi}$. Define a function $g(x)$, which gives the distance between x and its nearest $k\sqrt{\pi}$,

$$g(x) = x - k\sqrt{\pi}, \quad \text{for } (k - \frac{1}{2})\sqrt{\pi} \leq x < (k + \frac{1}{2})\sqrt{\pi}. \quad (11)$$

Our guess for the value of u is $g(q_2)$ and we apply a displacement $-g(q_2)$ to the data qubit to correct the error. With a high probability the displacement error can be corrected successfully, while sometimes the error correction procedure could introduce a large displacement error and therefore result in a logical Pauli error. Define the residual displacement of the GKP state after the SUM gate and feed forward as

$$u' = u - g(q_2) = u - g(u). \quad (12)$$

If $|u - 2k\sqrt{\pi}| < \sqrt{\pi}/2$, then $g(u) = u - 2k\sqrt{\pi}$ and $u' = u - (u - 2k\sqrt{\pi}) = 2k\sqrt{\pi}$, which means a stabilizer is applied to the GKP state and no error occurs. If $|u - (2k+1)\sqrt{\pi}| < \sqrt{\pi}/2$, then $g(u) = u - (2k+1)\sqrt{\pi}$ and $u' = u - [u - (2k+1)\sqrt{\pi}] = (2k+1)\sqrt{\pi}$, which means a stabilizer and a logical Pauli operator \bar{X} that flips the computational basis states are applied to the GKP state and a logical Pauli error occurs. We divide the displacement error in position space into two different zones, denoted as the Pauli error zone (PZ) and no Pauli error zone (NPZ), according to whether they lead to a logical Pauli error or not,

$$\begin{aligned} \text{PZ} &= \left\{ u : |u - (2k+1)\sqrt{\pi}| < \frac{\sqrt{\pi}}{2}, k \in \mathbb{Z} \right\}, \\ \text{NPZ} &= \left\{ u : |u - 2k\sqrt{\pi}| < \frac{\sqrt{\pi}}{2}, k \in \mathbb{Z} \right\}. \quad (13) \end{aligned}$$

For narrative convenience we define a serial number for PZ and NPZ,

$$\begin{aligned} \text{PZ}_m &= \left[\left(2m - \frac{m}{|m|} - \frac{1}{2}\right)\sqrt{\pi}, \left(2m - \frac{m}{|m|} + \frac{1}{2}\right)\sqrt{\pi} \right), \\ \text{NPZ}_m &= \left[2m\sqrt{\pi} - \frac{\sqrt{\pi}}{2}, 2m\sqrt{\pi} + \frac{\sqrt{\pi}}{2} \right), \quad (14) \end{aligned}$$

with $m \in \mathbb{Z}$. Note that PZ_0 is not defined for the sake of symmetry. The location of NPZ_m and PZ_m is shown in Fig. 3.

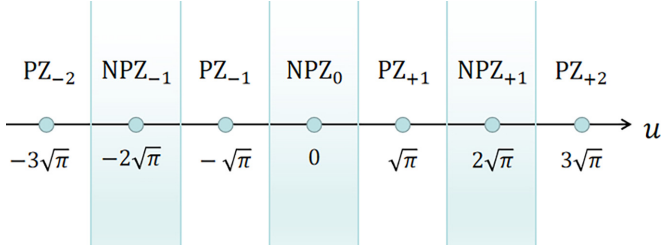


FIG. 3. Distribution of no Pauli error zone (NPZ) and Pauli error zone (PZ). PZ_0 is not defined for the sake of symmetry.

With these definitions the error correction procedure can be summarized as follows:

$$u \in \text{NPZ} \Rightarrow u' \pmod{2\sqrt{\pi}} = 0 \Rightarrow \text{perfect correction,}$$

$$u \in \text{PZ} \Rightarrow u' \pmod{2\sqrt{\pi}} = \sqrt{\pi} \Rightarrow \text{Pauli } \bar{X} \text{ error.}$$

The failure probability of error correction $P_{\bar{X}}$, which is also known as the logical Pauli \bar{X} error rate, is the probability that u falls in the PZ

$$\begin{aligned} P_{\bar{X}} &= \int_{\text{PZ}} f_q(u) du = \sum_{n=-\infty}^{+\infty} \int_{\sqrt{\pi}/2+2n\sqrt{\pi}}^{3\sqrt{\pi}/2+2n\sqrt{\pi}} f_q(u) du \\ &= \frac{1}{2} \sum_{n=-\infty}^{+\infty} \left[\text{erf}\left(\frac{4n+3}{2\Delta}\sqrt{\pi}\right) - \text{erf}\left(\frac{4n+1}{2\Delta}\sqrt{\pi}\right) \right]. \end{aligned} \quad (15)$$

The relation between $P_{\bar{X}}$ and Δ is plotted in Fig. 4. We can see that a smaller Δ , which corresponds to a higher degree of squeezing, leads to a lower logical Pauli \bar{X} error rate.

B. GKP error correction with finite-energy ancilla

We now consider a more realistic error correction procedure with finite-energy ancillary GKP qubits. We use the same GKP error correction circuit, as shown in Fig. 2, with the ancillary qubit prepared in a finite-energy GKP state. The SUM gate, which is designed for ideal GKP codes, distorts the envelopes of both the data and ancillary finite-energy GKP qubits [42], in particular, it increases the envelope width in position space for the ancillary qubit and that in momentum

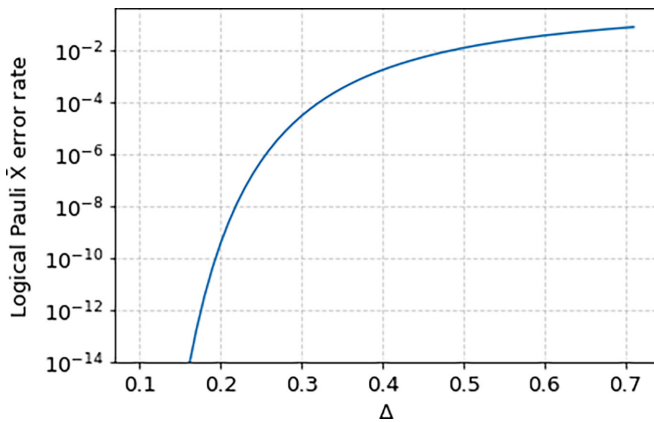


FIG. 4. Relation between the logical Pauli \bar{X} error rate and the standard deviation of the probability distribution of the finite-energy GKP state.

space for the data qubit. It is therefore advantageous to use the envelope-preserving SUM gate [43,44]. However, the accuracy of inferring the position displacement error of the data qubit depends on the peak width rather than the envelope width of the ancillary qubit. It is expected that the use of the ideal SUM gate would give the same logical error rate as the use of the envelope-preserving SUM gate. We therefore use the ideal SUM throughout the paper.

Suppose the variances of the data and ancillary qubit of the position quadrature are Δ^2 and $\tilde{\Delta}^2$, and the displacement errors in position space are u_1 and u_2 , respectively. The probability distribution of u_1 and u_2 are given by

$$f_{q_1}(u_1) = \frac{1}{\sqrt{\pi}\Delta} e^{-\frac{u_1^2}{\Delta^2}}, \quad f_{q_2}(u_2) = \frac{1}{\sqrt{\pi}\tilde{\Delta}} e^{-\frac{u_2^2}{\tilde{\Delta}^2}}. \quad (16)$$

According to the transformation rule of the SUM gate, one can show that the measurement outcome of the ancillary qubit is

$$q_2 = k\sqrt{\pi} + u_1 + u_2. \quad (17)$$

However, both u_1 and u_2 are unknown. By using the same procedure as before, we infer the true value of u_1 by subtracting from q_2 the nearest $k\sqrt{\pi}$. This means our guess for the error in the data qubit is $g(u_1 + u_2)$. This is not exactly the same as u_1 except that $u_2 = m\sqrt{\pi}$. However, this procedure is acceptable when u_2 is sufficiently small. We then apply a displacement $-g(u_1 + u_2)$ to the data qubit to correct its displacement error. The residual displacement in the data qubit is

$$\begin{aligned} u' &= u_1 - g(u_1 + u_2) = k\sqrt{\pi} - u_2, \\ &\text{for } (k - \frac{1}{2})\sqrt{\pi} \leq u_1 + u_2 < (k + \frac{1}{2})\sqrt{\pi}. \end{aligned} \quad (18)$$

It is evident that the residual displacement u' is continuous, contrary to the ideal case where u' is discrete. However, one can still define whether a logical Pauli error occurs or not. When u' is close to $2k\sqrt{\pi}$, no logical Pauli error occurs; when u' is close to $(2k+1)\sqrt{\pi}$, a Pauli \bar{X} error occurs.

To understand the error correcting property with finite-energy ancillary qubit and to evaluate the logical Pauli error rate, one needs to compute the probability distribution of u' , which is given by (see Appendix B for details)

$$\begin{aligned} F(u') &= \frac{1}{2\sqrt{\pi}\tilde{\Delta}} \left[\text{erf}\left(\frac{u' + \frac{\sqrt{\pi}}{2}}{\Delta}\right) - \text{erf}\left(\frac{u' - \frac{\sqrt{\pi}}{2}}{\Delta}\right) \right] \\ &\times \sum_t \exp\left[-\frac{(u' - t\sqrt{\pi})^2}{\tilde{\Delta}^2}\right]. \end{aligned} \quad (19)$$

We can see that $F(u')$ is determined by a modulating term $\text{erf}[(u' + \sqrt{\pi}/2)/\Delta] - \text{erf}[(u' - \sqrt{\pi}/2)/\Delta]$ and a wave packet term $\sum_t \exp[-\frac{(u' - t\sqrt{\pi})^2}{\tilde{\Delta}^2}]$. The first is determined by the degree of squeezing of the data qubit, while the second is determined by the degree of squeezing of the ancillary qubit.

To have an intuitive feeling of the probability distribution, we plot several examples of $F(u')$ in Fig. 5. It can be seen that the distribution has a high peak at $u' = 0$ and two low peaks that are located symmetrically with respect to $u' = 0$. The peaks outside the $PZ_{\pm 1}$ are strongly suppressed by the modulating term, so the residual displacement outside the $PZ_{\pm 1}$ can be neglected. Additionally, a smaller $\tilde{\Delta}$ leads to

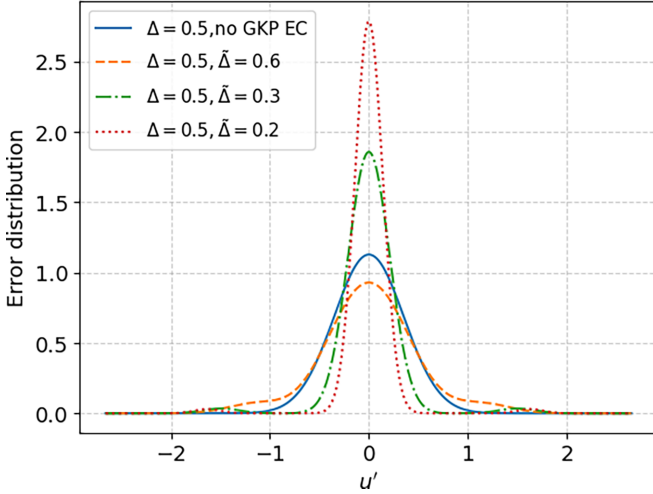


FIG. 5. Error distribution of GKP state after error correction with a finite-energy ancillary qubit. We choose $\Delta = 0.5$ and compare results with several different $\tilde{\Delta}$. The peaks outside $\text{PZ}_{\pm 1}$ are strongly suppressed and a smaller $\tilde{\Delta}$ leads to a narrower peak in NPZ_0 , indicating a better correction to the small displacement error.

a narrower distribution of u' in the NPZ_0 , showing a better performance of error correction. This can be understood in an intuitive way: error correction using the SUM gate is basically substituting the error of the data qubit by the error of the ancillary qubit, hence an ancillary qubit with higher quality naturally leads to a better performance of error correction. If the ancillary qubit is ideal, i.e., $\tilde{\Delta} = 0$, then the distribution of u' approaches to a delta function, which means the state can be perfectly corrected.

The error correction is successful when u' is in NPZ and fails when u' is in PZ . Therefore, the failure probability of error correction, namely, the logical Pauli error rate is given by

$$P_F(\Delta, \tilde{\Delta}) = \sum_{n=-\infty}^{+\infty} \int_{\sqrt{\pi}/2+2n\sqrt{\pi}}^{3\sqrt{\pi}/2+2n\sqrt{\pi}} F(u') du' \approx 2 \int_{\sqrt{\pi}/2}^{3\sqrt{\pi}/2} F(u') du'. \quad (20)$$

The relation between $P_F(\Delta, \tilde{\Delta})$ and $\tilde{\Delta}$ for a fixed Δ is plotted in Fig. 6. We can see that P_F monotonically decreases as $\tilde{\Delta}$ decreases, showing that an ancillary GKP qubit with higher quality naturally leads to lower logical Pauli error rate. In addition, it can be shown that

$$P_F(\Delta, \tilde{\Delta} \rightarrow 0) = P_{\tilde{X}}(\Delta). \quad (21)$$

It is an important property that error correction by SUM gate with a finite-energy ancillary qubit always increases logical Pauli error rate as compared to that with an ideal ancillary qubit. In the case of ideal ancillary qubit, a logical Pauli error occurs when $u_1 \in \text{PZ}$ and no error occurs when $u_1 \in \text{NPZ}$. While in the case of finite-energy ancillary qubit, $u_1 \in \text{NPZ}$ may lead to a logical Pauli error because of the presence of an additional displacement u_2 . Although $u_1 \in \text{PZ}$ may not lead to a logical Pauli error due to the same reason, its probability is much less than the previous one.

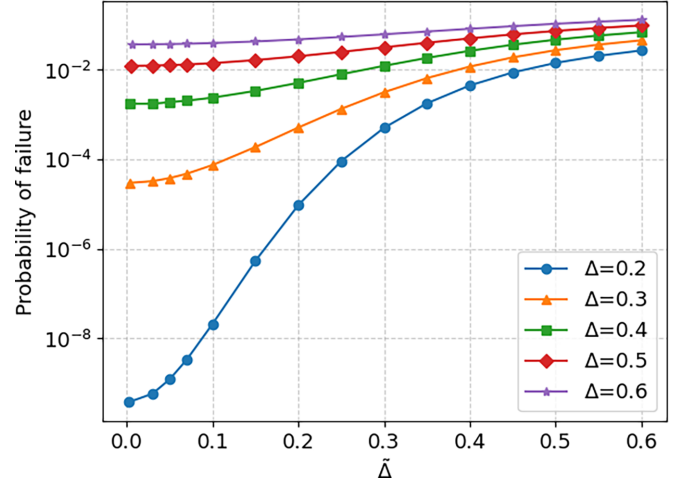


FIG. 6. Relation between the failure probability $P_F(\Delta, \tilde{\Delta})$ with finite-energy ancillary qubit and $\tilde{\Delta}$, with Δ fixed for each curve.

IV. CONCATENATION WITH REPETITION CODE

In the previous section, we discuss GKP error correction with ideal and finite-energy ancillary GKP qubits, and find that small displacement error can be effectively corrected. The logical Pauli error rate with finite-energy ancillary GKP qubits is generally higher than that with ideal ancillary GKP qubits. To further suppress the logical Pauli error, we concatenate the GKP code with repetition code [40,45,46]. Note that by concatenating with the repetition code we only correct the displacement error in position space.

A. Concatenation with three-qubit repetition code

The repetition code is a kind of error-correcting code realized by redundancy encoding (see Appendix C for details if you are not familiar with classical repetition code). To concatenate the GKP code with repetition code, one needs to replace the standard qubits by the GKP qubits and find a CV gate that corresponds to the CNOT gate. It turns out that the SUM gate we used to perform GKP error correction plays the role as a CNOT gate. The quantum circuit of encoding is shown in Fig. 7, which is a generalization of the encoding circuit for repetition code. Before encoding, the first GKP qubit is prepared in the state $|\xi\rangle = \alpha|\bar{0}\rangle + \beta|\bar{1}\rangle$, and the other two data qubits are prepared in the same state $|\xi_1\rangle = |\xi_2\rangle = |\bar{0}\rangle$.

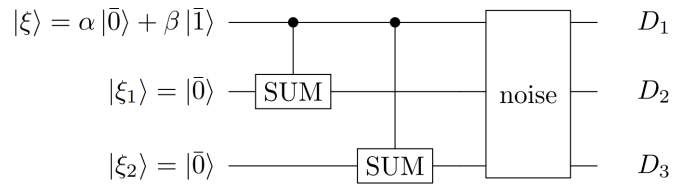


FIG. 7. Quantum circuit of encoding for three-qubit GKP repetition code. The three GKP states before encoding are assumed to be ideal. After the encoding, three data qubits entangle with each other. A finite-energy GKP repetition code state is constructed by coherently superposing the ideal GKP states undergoing random displacements.

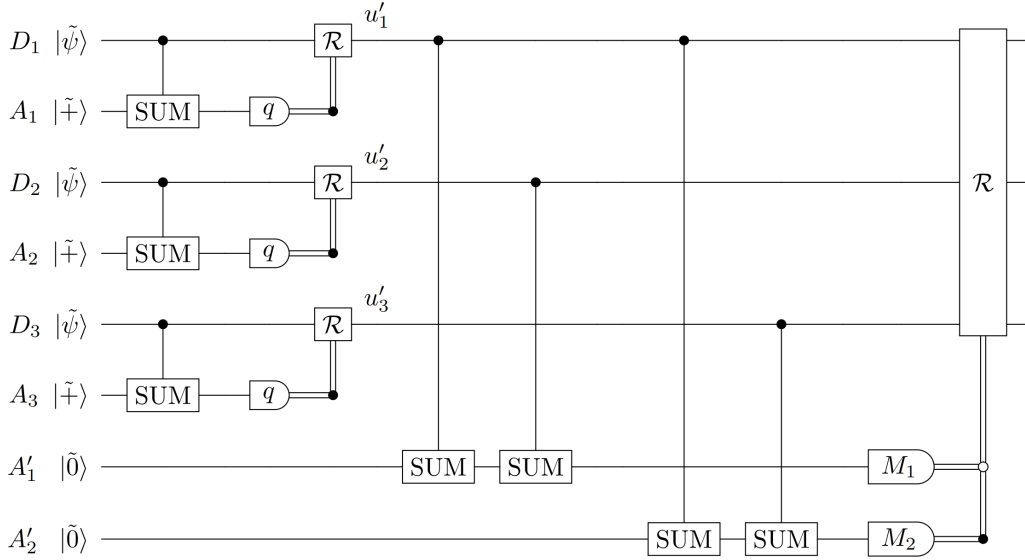


FIG. 8. Quantum error correction circuit of three-qubit GKP repetition code. It consists of one round of GKP error correction, syndrome measurement of repetition code, and recovery operation according to the measurement outcomes M_1 and M_2 . Three data qubits D_1 , D_2 , and D_3 are all finite-energy GKP states with noise variance Δ^2 in position quadrature. Ancillary qubits A_1 , A_2 , and A_3 are prepared in the state $|\tilde{+}\rangle$, ancillary qubits A'_1 and A'_2 are prepared in the state $|\tilde{0}\rangle$, and we assume noise variances in position quadrature of all ancillary qubits to be $\tilde{\Delta}^2$. Residual displacements of three data qubits D_1 , D_2 , and D_3 after the GKP error correction are denoted as u'_1 , u'_2 , and u'_3 , respectively.

After the encoding procedure, namely, the application of two SUM gates, three GKP states become entangled with each other

$$\begin{aligned} |\xi, \xi_1, \xi_2\rangle &= (\alpha |\tilde{0}\rangle + \beta |\tilde{1}\rangle) |\tilde{0}\rangle |\tilde{0}\rangle \rightarrow |\tilde{\psi}_3\rangle \\ &= \alpha |\tilde{0}\tilde{0}\tilde{0}\rangle + \beta |\tilde{1}\tilde{1}\tilde{1}\rangle. \end{aligned} \quad (22)$$

The state $|\tilde{\psi}_3\rangle$ as defined is an ideal GKP repetition code state. One way to construct a finite-energy GKP repetition code state is to coherently superpose the randomly displaced ideal GKP repetition code states, namely,

$$\begin{aligned} |\tilde{\Psi}_3\rangle &= \int du_1 dv_1 du_2 dv_2 du_3 dv_3 \eta(u_1, v_1) \eta(u_2, v_2) \\ &\quad \times \eta(u_3, v_3) e^{i(-u_1 \hat{p}_1 + v_1 \hat{q}_1)} e^{i(-u_2 \hat{p}_2 + v_2 \hat{q}_2)} e^{i(-u_3 \hat{p}_3 + v_3 \hat{q}_3)} |\tilde{\psi}_3\rangle. \end{aligned} \quad (23)$$

Here we assume that the displacement in each ideal GKP qubit is independent and follows the same probability distribution. This definition of the finite-energy code state is similar to the definition of a single-qubit finite-energy GKP state in Eq. (2). The GKP repetition code state defined in Eq. (23) is different from the state generated by applying two SUM gates to three single-qubit finite-energy GKP states, since the second of these would generate correlated noise between different GKP qubits. We use the GKP repetition code state (23) only to seek convenience for calculation, and we will leave the discussion on its experimental preparation for future work.

Error correction is performed after the encoding, which is implemented by the quantum circuit shown in Fig. 8. The full process of error correction consists of three steps: one round of GKP error correction, syndrome measurement and feed forward based on the measurement outcome. The three data GKP qubits, denoted as D_1 , D_2 , D_3 , have finite energy and their noise variances of the position quadrature are the

same, which is assumed to be Δ^2 . Three ancillary GKP qubits, denoted as A_1 , A_2 , and A_3 , are introduced to perform the GKP error correction, and they are prepared in the GKP $|\tilde{+}\rangle$ state. Another two ancillary GKP qubits, denoted as A'_1 and A'_2 , are introduced to perform the syndrome measurement, and they are prepared in the GKP $|\tilde{0}\rangle$ state. The noise variances of the position quadrature of all ancillary GKP qubits are assumed to be the same and is $\tilde{\Delta}^2$. The residual displacements of the three data qubits after the GKP error correction are denoted as u'_1 , u'_2 , u'_3 , respectively. Their probability distribution is given by Eq. (19). Denote the displacement errors of the ancillary qubits A'_1 and A'_2 as α_1 and α_2 , respectively, whose probability distribution is given by

$$f_{q_i}(\alpha_i) = \frac{1}{\sqrt{\pi} \tilde{\Delta}} e^{-\frac{\alpha_i^2}{\tilde{\Delta}^2}}, \quad i = 1, 2. \quad (24)$$

The purpose of the syndrome measurement is to compare the states of three data GKP qubits, which is implemented by applying four SUM gates that act on the data qubits and the ancillary qubits in an appropriate way, as shown in Fig. 8. After these SUM gates, the displacement errors of the ancillary qubits A'_1 and A'_2 become $u'_1 + u'_2 + \alpha_1$ and $u'_1 + u'_3 + \alpha_2$, respectively. Then measurement of the ancillary qubits A'_1 and A'_2 gives $M_1 = 2k_1 \sqrt{\pi} + u'_1 + u'_2 + \alpha_1$ and $M_2 = 2k_2 \sqrt{\pi} + u'_1 + u'_3 + \alpha_2$, with $k_1 \in \mathbb{Z}$ and $k_2 \in \mathbb{Z}$.

The way to identify the bit-flip error through the syndrome in three-qubit GKP repetition code is similar to that of three-qubit repetition code (see Appendix C). The correspondence between measurement outcomes $\{M_1, M_2\}$ and the logical Pauli \tilde{X} error on different GKP qubits is summarized in Table I. However, this decoding procedure has a subtle difference from that of the repetition code: sometimes a single-qubit Pauli \tilde{X} error could be

misidentified. As an example, if $u'_1 = \sqrt{\pi} \in \text{PZ}$, $u'_2 = \sqrt{\pi}/3 \in \text{NPZ}$, $u'_3 = \sqrt{\pi}/3 \in \text{NPZ}$, $\alpha_1 = \alpha_2 = \sqrt{\pi}/3$, then $M_1 = 2k_1\sqrt{\pi} + u'_1 + u'_2 + \alpha_1 = 2k_1\sqrt{\pi} + 5\sqrt{\pi}/3 \in \text{NPZ}$, $M_2 = 2k_2\sqrt{\pi} + u'_1 + u'_3 + \alpha_2 = 2k_2\sqrt{\pi} + 5\sqrt{\pi}/3 \in \text{NPZ}$, from which we infer that no Pauli \bar{X} error occurs but in fact a Pauli \bar{X} error did occur in the qubit D_1 . Continuity of the

phase space is what makes GKP repetition code different from the classical repetition code [45].

Considering all the circumstances where decoding procedures fail, we can give the total failure probability of the three-qubit GKP repetition code as follows (see Appendix D for details):

$$P_{f,3\text{-rep}}(\Delta, \tilde{\Delta}) = P_{f,3\text{-rep}}^1 + P_{f,3\text{-rep}}^2 + P_{f,3\text{-rep}}^3 + P_{f,3\text{-rep}}^4 + P_{f,3\text{-rep}}^5$$

$$\approx \int_{u'_1=-\sqrt{\pi}/2}^{\sqrt{\pi}/2} \int_{u'_2=-\sqrt{\pi}/2}^{\sqrt{\pi}/2} \int_{u'_3=-\sqrt{\pi}/2}^{\sqrt{\pi}/2} F(u'_1, u'_2, u'_3) [1 - P_\alpha^1(u'_1, u'_2, u'_3)] du'_1 du'_2 du'_3$$

$$+ 6 \int_{u'_1=\sqrt{\pi}/2}^{3\sqrt{\pi}/2} \int_{u'_2=-\sqrt{\pi}/2}^{\sqrt{\pi}/2} \int_{u'_3=-\sqrt{\pi}/2}^{\sqrt{\pi}/2} F(u'_1, u'_2, u'_3) [1 - P_\alpha^2(u'_1, u'_2, u'_3)] du'_1 du'_2 du'_3 + 3P_F^2(1 - P_F) + P_F^3, \quad (25)$$

where

$$P_\alpha^1(u'_1, u'_2, u'_3) \approx \frac{1}{4} \left[\text{erf}\left(\frac{\frac{\sqrt{\pi}}{2} - u'_1 - u'_2}{\tilde{\Delta}}\right) - \text{erf}\left(\frac{-\frac{\sqrt{\pi}}{2} - u'_1 - u'_2}{\tilde{\Delta}}\right) \right] \left[\text{erf}\left(\frac{\frac{\sqrt{\pi}}{2} - u'_1 - u'_3}{\tilde{\Delta}}\right) - \text{erf}\left(\frac{-\frac{\sqrt{\pi}}{2} - u'_1 - u'_3}{\tilde{\Delta}}\right) \right],$$

and

$$P_\alpha^2(u'_1, u'_2, u'_3) \approx \frac{1}{4} \left[\text{erf}\left(\frac{\frac{3\sqrt{\pi}}{2} - u'_1 - u'_2}{\tilde{\Delta}}\right) - \text{erf}\left(\frac{\frac{\sqrt{\pi}}{2} - u'_1 - u'_2}{\tilde{\Delta}}\right) \right] \left[\text{erf}\left(\frac{\frac{3\sqrt{\pi}}{2} - u'_1 - u'_3}{\tilde{\Delta}}\right) - \text{erf}\left(\frac{\frac{\sqrt{\pi}}{2} - u'_1 - u'_3}{\tilde{\Delta}}\right) \right],$$

and $F(u'_1, u'_2, u'_3) = F(u'_1)F(u'_2)F(u'_3)$. The last two terms correspond to the failure probability of the classical three-qubit repetition code, and the first two terms correspond to the failure probability when error occurs on no more than one data qubit, which is what makes GKP repetition code different from the classical repetition code.

The relation between the failure probability $P_{f,3\text{-rep}}(\Delta, \tilde{\Delta})$ and $\tilde{\Delta}$ for $\Delta = 0.5$ is shown in Fig. 9, in which $P_F(\Delta, \tilde{\Delta})$ is also included for comparison. From Fig. 9 we can see that $P_{f,3\text{-rep}}(\Delta, \tilde{\Delta})$ is monotonically decreasing as $\tilde{\Delta}$ decreases. This implies that ancillary qubits with higher quality lead to a lower logical Pauli error rate. When $\tilde{\Delta} \rightarrow 0$, the logical Pauli error rate approaches to that of the classical three-qubit repetition code, namely,

$$P_{f,3\text{-rep}}(\Delta, \tilde{\Delta} \rightarrow 0) = 3P_{\bar{X}}^2(\Delta)[1 - P_{\bar{X}}(\Delta)] + P_{\bar{X}}^3(\Delta)$$

$$= P_{f,3\text{-rep}}^{\text{class}}(\Delta). \quad (26)$$

This can be understood as follows. The probability distribution of $u'_1, u'_2, u'_3, \alpha_1$, and α_2 are determined by $\tilde{\Delta}$, and when $\tilde{\Delta} \rightarrow 0$ the distribution is highly localized and is close to a

δ function. As a result, the probability of misidentifying no error and single-qubit Pauli \bar{X} errors is almost zero. When $\tilde{\Delta}$ is large, the failure probability $P_{f,3\text{-rep}}(\Delta, \tilde{\Delta})$ is greater than $P_F(\Delta, \tilde{\Delta})$. However, the first decreases faster than the second as $\tilde{\Delta}$ decreases. There exists a critical value for $\tilde{\Delta}$, denoted as $\tilde{\Delta}_{\text{cr}}$, such that $P_{f,3\text{-rep}}(0.5, \tilde{\Delta}_{\text{cr}}) = P_F(0.5, \tilde{\Delta}_{\text{cr}})$, and from Fig. 9 we can see that $\tilde{\Delta}_{\text{cr}} \approx 0.3$. When $\tilde{\Delta} < \tilde{\Delta}_{\text{cr}}$, the logical Pauli error rate of the three-qubit GKP repetition code is lower

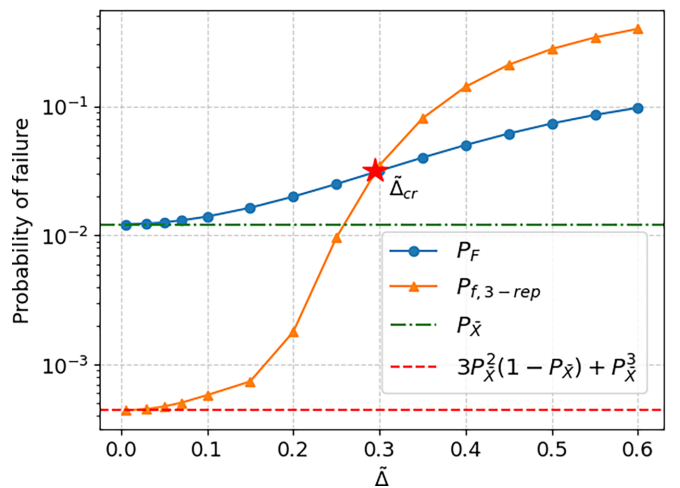


FIG. 9. Comparison of logical Pauli error rate $P_{f,3\text{-rep}}(\Delta, \tilde{\Delta})$ and $P_F(\Delta, \tilde{\Delta})$ for a fixed Δ , where we choose $\Delta = 0.5$ as an example. When $\tilde{\Delta} \rightarrow 0$, the failure probability of the three-qubit GKP repetition code approaches to that of the classical three-qubit repetition code. There exists a critical value at $\tilde{\Delta} = \tilde{\Delta}_{\text{cr}}$, below which $P_{f,3\text{-rep}}(\Delta, \tilde{\Delta}) < P_F(\Delta, \tilde{\Delta})$ and above which $P_{f,3\text{-rep}}(\Delta, \tilde{\Delta}) > P_F(\Delta, \tilde{\Delta})$.

TABLE I. Correspondence between syndromes and single-qubit bit-flip errors for the three-qubit GKP repetition code. The syndromes are defined according to whether M_1 and M_2 belong to PZ or NPZ.

Measurement outcome	Error
$M_1 \in \text{NPZ}, M_2 \in \text{NPZ}$	No error
$M_1 \in \text{PZ}, M_2 \in \text{PZ}$	\bar{X} on data qubit 1
$M_1 \in \text{PZ}, M_2 \in \text{NPZ}$	\bar{X} on data qubit 2
$M_1 \in \text{NPZ}, M_2 \in \text{PZ}$	\bar{X} on data qubit 3

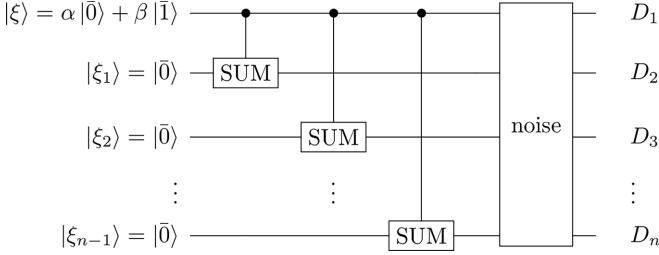


FIG. 10. Encoding circuit for n -qubit GKP repetition code. The n GKP states before encoding are assumed to be ideal. After encoding, n data qubits entangle with each other. Then a finite-energy GKP n -qubit repetition code state is constructed by coherently superposing the ideal GKP states undergoing random displacements.

than that of the GKP code with finite-energy ancillary qubits. The concatenation with repetition code, therefore, shows its advantage in this regime. Furthermore, the failure probability $P_{f,3\text{-rep}}(\Delta, \tilde{\Delta})$ can be even lower than that of the GKP code with ideal ancillary qubits, namely, $P_{f,3\text{-rep}}(0.5, \tilde{\Delta}) < P_{\tilde{\chi}}(0.5)$.

B. Concatenation with n -qubit repetition code

In the theory of quantum error correction, introducing more qubits would allow more errors to be corrected and therefore achieve a lower logical error rate [1–3]. In this section, we generalize the previous scheme and concatenate the GKP code with n -qubit repetition code, with n an odd integer. We are going to show that increasing the size of the GKP repetition code can further reduce the logical Pauli error rate, though one needs to prepare ancillary GKP qubits with higher quality. We now concatenate the GKP code with the n -qubit repetition code. The quantum circuit of encoding is shown in Fig. 10, where we assume all input GKP states are ideal. Before encoding, the first GKP qubit is prepared in the state $\alpha|\bar{0}\rangle + \beta|\bar{1}\rangle$, and all other GKP qubits are prepared in the state $|\bar{0}\rangle$. After the

encoding procedure, namely, the application of $(n - 1)$ SUM gates, the n GKP qubits become entangled with each other,

$$|\xi, \xi_1, \xi_2, \dots, \xi_{n-1}\rangle \rightarrow |\tilde{\psi}_n\rangle = \alpha|\bar{0}\bar{0}\bar{0}\dots\bar{0}\rangle + \beta|\bar{1}\bar{1}\bar{1}\dots\bar{1}\rangle. \quad (27)$$

We then construct a finite-energy GKP repetition code state by coherently superposing the randomly displaced ideal GKP repetition code states, namely,

$$|\tilde{\Psi}_n\rangle = \int du_1 dv_1 \dots du_n dv_n \eta(u_1, v_1) \dots \eta(u_n, v_n) \times \exp\left\{-i \sum_{k=1}^n (u_k \hat{p}_k - v_k \hat{q}_k)\right\} |\tilde{\psi}_n\rangle. \quad (28)$$

We assume that the displacement in each ideal GKP qubit is independent and follows the same probability distribution.

The quantum circuit of error correction is shown in Fig. 11, which is a direct generalization to that of the three-qubit GKP repetition code, and the procedure of quantum error correction is also similar. The residual displacements of the n data qubits after the GKP error correction are denoted as $\{u'_i\}_{i=1}^n$, and their probability distribution is given by Eq. (19). The displacement errors of the $(n - 1)$ ancillary qubits for syndrome measurement are denoted as $\{\alpha'_i\}_{i=1}^{n-1}$, and their probability distribution is given by Eq. (24). The outcomes of the syndrome measurement are given by

$$M_i = 2k_i\sqrt{\pi} + u'_1 + u'_{i+1} + \alpha'_i, \quad i = 1, 2, \dots, n - 1, \quad (29)$$

with $k_i \in \mathbb{Z}$. Similarly, there is a one-to-one correspondence between the syndromes and correctable errors, which is summarized in Table II.

Using the same method, we can calculate the failure probability of the n -qubit GKP repetition code (see Appendix E for details). We calculate the failure probability $P_{f,n\text{-rep}}(\Delta, \tilde{\Delta})$ for the GKP repetition code with the number of data qubits up to $n = 9$. The results for a fixed Δ are shown in Fig. 12, in which we choose $\Delta = 0.5$ as an example. First, it can be seen that

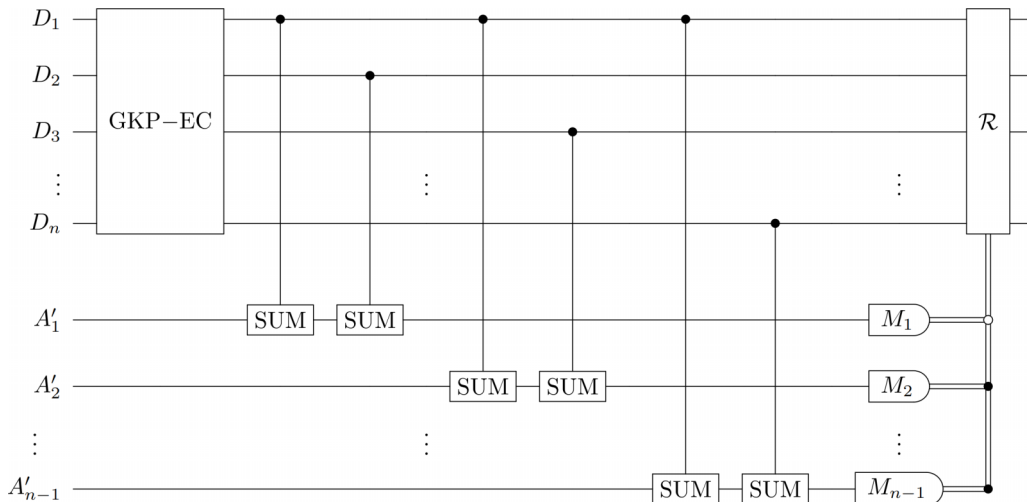


FIG. 11. Quantum error correction circuit for n -qubit GKP repetition code. It consists of one round of GKP error correction, syndrome measurement of repetition code, and recovery operation according to the measurement outcomes $\{M_i\}_{i=1}^{n-1}$. Here $\{D_i\}_{i=1}^n$ denote the data qubits and $\{A'_i\}_{i=1}^{n-1}$ denote the ancillary qubits introduced to perform syndrome measurement.

TABLE II. Correspondence between syndromes and single-qubit bit-flip errors for the n -qubit GKP repetition code.

Measurement outcome	Error
$M_1, M_2, \dots, M_{n-1} \in \text{NPZ}$	No error
$M_1, M_2, \dots, M_{n-1} \in \text{PZ}$	D_1
$M_1 \in \text{PZ}, M_2, \dots, M_{n-1} \in \text{NPZ}$	D_2
$M_1 \in \text{NPZ}, M_2 \in \text{PZ}, M_3, \dots, M_{n-1} \in \text{NPZ}$	D_3
.....
$M_1 \in \text{NPZ}, M_2, \dots, M_{n-1} \in \text{PZ}$	D_1, D_2
$M_1 \in \text{PZ}, M_2 \in \text{NPZ}, M_3, \dots, M_{n-1} \in \text{PZ}$	D_1, D_3
.....
$M_1, M_2 \in \text{NPZ}, M_3, \dots, M_{n-1} \in \text{PZ}$	D_1, D_2, D_3
.....

the failure probability $P_{f,n\text{-rep}}(\Delta, \tilde{\Delta})$ for all n monotonically decreases as $\tilde{\Delta}$ decreases. This implies that ancillary qubits with higher quality lead to a lower logical Pauli error rate. In the limit of $\tilde{\Delta} \rightarrow 0$, the logical Pauli error rate approaches to that of the classical n -qubit repetition code, namely,

$$P_{f,n\text{-rep}}(\Delta, \tilde{\Delta} \rightarrow 0) = \sum_{i=\frac{n+1}{2}}^n C_n^i P_X^i(\Delta) [1 - P_X(\Delta)]^{n-i} = P_{f,n\text{-rep}}^{\text{class}}(\Delta). \quad (30)$$

The second observation is that when $\tilde{\Delta}$ is sufficiently large, the logical Pauli error rate increases as the size of the code increases; when $\tilde{\Delta}$ is sufficiently small, the logical Pauli error rate decreases as the size of the code increases. This implies that the concatenation of GKP code with repetition code can reduce the logical Pauli error rate under the condition that the quality of the ancillary qubit is sufficiently high. Figure 12 indicates that there exists some threshold for $\tilde{\Delta}$, below which the concatenation shows advantages. However, the location of the threshold is not sharp. Define the critical noise variance $\tilde{\Delta}_{nm}^2$ as the variance of the ancillary qubit when the

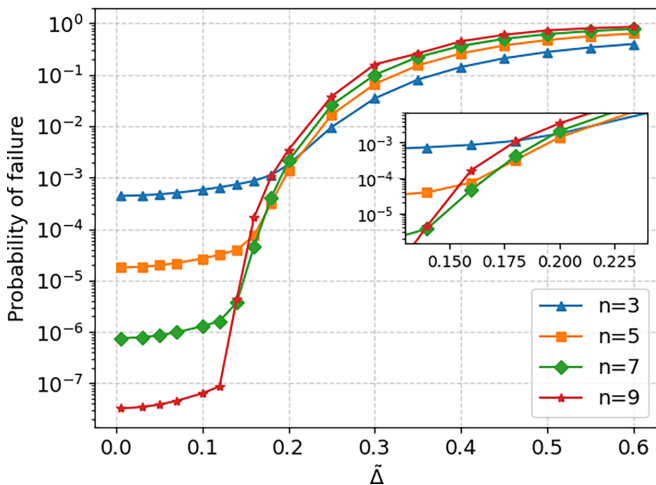


FIG. 12. Comparison of logical Pauli error rate $P_{f,n\text{-rep}}(\Delta, \tilde{\Delta})$ of n -qubit GKP repetition codes for n from 3 to 9, with $\Delta = 0.5$ as an example. The inset shows the location of various critical values.

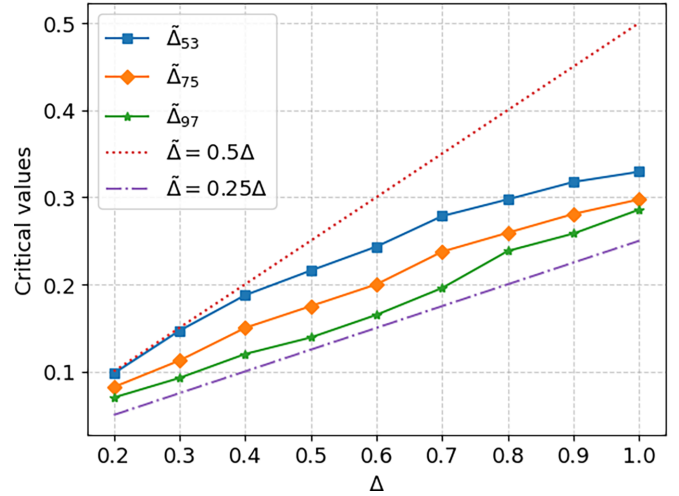


FIG. 13. Relation between $\tilde{\Delta}_{nm}$ and Δ . The ratio $\tilde{\Delta}_{nm}/\Delta$ is upper bounded by 0.5 and lower bounded by 0.25 for the code size n from 3 to 9.

n -qubit GKP repetition code and the m -qubit GKP repetition code have the same logical Pauli error rate for a fixed Δ . From Fig. 12 it can be seen that $\tilde{\Delta}_{97} < \tilde{\Delta}_{75} < \tilde{\Delta}_{53}$. They are close but not the same. When $\Delta > \tilde{\Delta}_{53}$, we have $P_{f,9\text{-rep}} > P_{f,7\text{-rep}} > P_{f,5\text{-rep}} > P_{f,3\text{-rep}}$. Therefore, $\tilde{\Delta}_{53}^2$ can be considered as the minimal noise variance that the concatenation with repetition code is completely useless. When $\tilde{\Delta} < \tilde{\Delta}_{97}$, we have $P_{f,9\text{-rep}} < P_{f,7\text{-rep}} < P_{f,5\text{-rep}} < P_{f,3\text{-rep}}$. Therefore, $\tilde{\Delta}_{97}^2$ is the noise variance that one needs to achieve to realize the power of repetition code concatenation with at least nine GKP qubits.

The critical noise variance $\tilde{\Delta}_{nm}^2$ depends on the noise variance of the data qubits. The relation between $\tilde{\Delta}_{nm}$ and Δ is shown in Fig. 13. We can see that $\tilde{\Delta}_{nm}$ increases monotonically as Δ increases. This implies that a lower-quality GKP repetition code requires lower quality ancillary qubits to achieve its advantage. This is rather surprising and counter-intuitive. However, one should keep in mind that this does not imply that a low-quality GKP repetition code is preferred in the experimental realization. This is because one also needs to take into account the displacement error in momentum space, which we will discuss later in Sec. V. From Fig. 13 it can be seen that the relation between $\tilde{\Delta}_{nm}$ and Δ is almost linear, we therefore define an approximate ratio $\tilde{\Delta}_{nm}/\Delta$ (or an average ratio). The ratio depends on the size of the code, and is upper bounded by 0.5 and lower bounded by 0.25 for the code size that we consider. This means if we choose $\tilde{\Delta} = 0.5\Delta$, the logical Pauli error rate increases as the size of the code increases, implying that concatenation with repetition code is useless; while if we choose $\tilde{\Delta} = 0.25\Delta$, the logical Pauli error rate decreases as the size of the code increases, implying that concatenation with repetition code with at least nine GKP qubits is useful.

We are not able to calculate the failure probability for arbitrarily large n since it involves a very high-dimensional integral, which is a rather challenging task. Based on the results with n up to nine, we conjecture that there exists a nonzero threshold for $\tilde{\Delta}$ such that for sufficiently small Δ the logical Pauli error rate can be exponentially suppressed by increasing

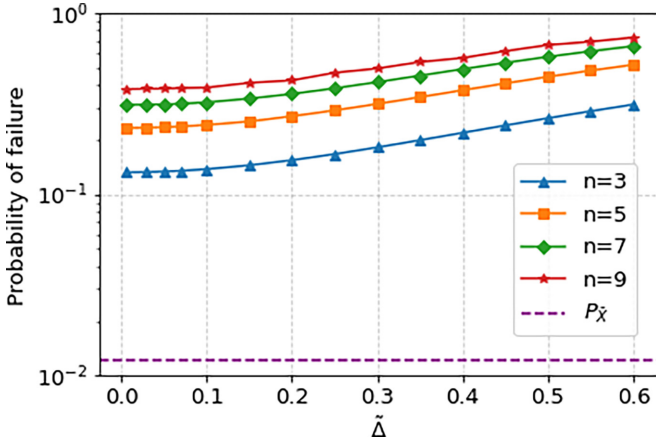


FIG. 14. Failure probabilities for GKP repetition codes without one round of GKP error correction before concatenation. Here we choose $\Delta = 0.5$.

the size of the code. This threshold can be calculated by using the Monte Carlo simulation and we leave it for future work.

C. Comparison with no GKP error correction

Although the GKP error correction increases the probability of Pauli \bar{X} error for all values of $\tilde{\Delta}$, it narrows down the error distribution of the GKP state when $\tilde{\Delta} < \Delta$ such that the concatenation with repetition code is advantageous. However, the GKP error correction requires the same number of ancillary GKP qubits as the data qubits. A question arises as to whether the GKP error correction is necessary to reduce the logical Pauli error rate. If the GKP error correction is not necessary, then we only need to supply ancillary GKP qubits for syndrome measurement and therefore can save a substantial amount of physical resources.

We calculate the failure probability $P'_{f,n\text{-rep}}(\Delta, \tilde{\Delta})$ for the GKP repetition code without one round of GKP error correction, with the number of data qubits up to $n = 9$ (see Appendix F for details). The results for a fixed Δ are shown in Fig. 14, in which we choose $\Delta = 0.5$ as an example. We can see that GKP repetition code without one round of GKP error correction cannot reduce the logical Pauli error rate even when $\tilde{\Delta} \rightarrow 0$, and increasing the size of the code leads to a higher logical Pauli error rate. We confirm that this is true for $\Delta \geq 0.2$, and we expect that this should also be the case when $\Delta < 0.2$. This is in contrast to the GKP repetition code with one round of GKP error correction, for which increasing the code size can lead to a lower logical Pauli error rate, as shown in Fig. 12. Therefore, one round of GKP error correction before concatenation is necessary.

V. BIASED NOISE CORRECTED BY GKP REPETITION CODE

Until now we have only considered correcting displacement errors in position space and neglected those in momentum space. Therefore, previous results are only valid in the limit of no errors in momentum space. However, a finite-energy GKP state does have noise in both position and momentum spaces. In this section, we take into account the

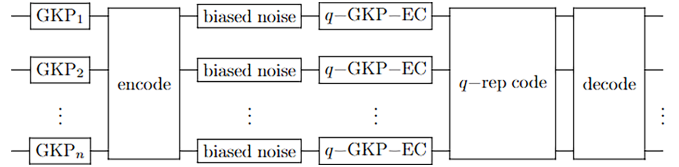


FIG. 15. Scheme to correct biased noise using GKP repetition code. Ideal GKP repetition code is first generated by injecting ideal GKP states into the encoding circuit. Biased noise is then imposed to the ideal GKP repetition code to produce a finite-energy GKP repetition code. The error correction consists of one round of GKP error correction, syndrome measurement on repetition code, and decoding.

effects of momentum displacement error and assume a biased noise model, namely, with unequal position and momentum noise, and introduce a GKP repetition code to suppress the logical error. Note that concatenating with repetition code does not correct momentum displacement error. We assume the momentum displacement error is suppressed when the GKP states are generated and by going through an anisotropic GDC. Equivalently, one considers isotropic noise and uses an anisotropic GKP code [40] in which the spacing between two adjacent peaks in momentum space is stretched, to effectively suppress the momentum displacement error.

The scheme of correcting biased noise using GKP repetition code is schematically shown in Fig. 15, where “q-GKP-EC” represents GKP error correction in position space, “q-rep code” represents error correction in position space by concatenating with the repetition code. The GKP states before encoding are assumed to be ideal. Biased noise is imposed to the data qubits after encoding, with the error probability distribution given by Eq. (6). By choosing $r > 1$, the error in momentum space is suppressed at the expense of amplifying the error in position space. Fortunately, this is not a problem because the displacement error in position space can be efficiently corrected by concatenating the GKP code with repetition code.

However, it should be noted that further error correction in position space will contaminate the momentum quadrature. After applying the SUM gate, the momentum displacement error of the ancillary qubits can propagate to the momentum space of the data qubits, therefore, the variance of the error distribution in momentum space will be amplified. The initial noise variance of the finite-energy GKP state in momentum space is $(\Delta/r)^2$. After one round of GKP error correction, the momentum displacement error of the ancillary GKP qubit propagates to the data qubit, resulting in a noise variance $(\Delta/r)^2 + \tilde{\Delta}^2$. Concatenation with the repetition code will further increase the noise in momentum space because of the sequential application of SUM gates during the syndrome measurement. By concatenating with an n -qubit repetition code, the noise variance of the first data qubit in momentum space becomes $(\Delta/r)^2 + n\tilde{\Delta}^2$ since it couples with $(n-1)$ ancillary qubits via the SUM gate; while the noise variance of all other data qubits in momentum space becomes $(\Delta/r)^2 + 2\tilde{\Delta}^2$ since each of them couples with only one ancillary qubit.

The logical information is protected when the momentum displacement is in NPZ and the correction of the position displacement using the GKP repetition code succeeds.

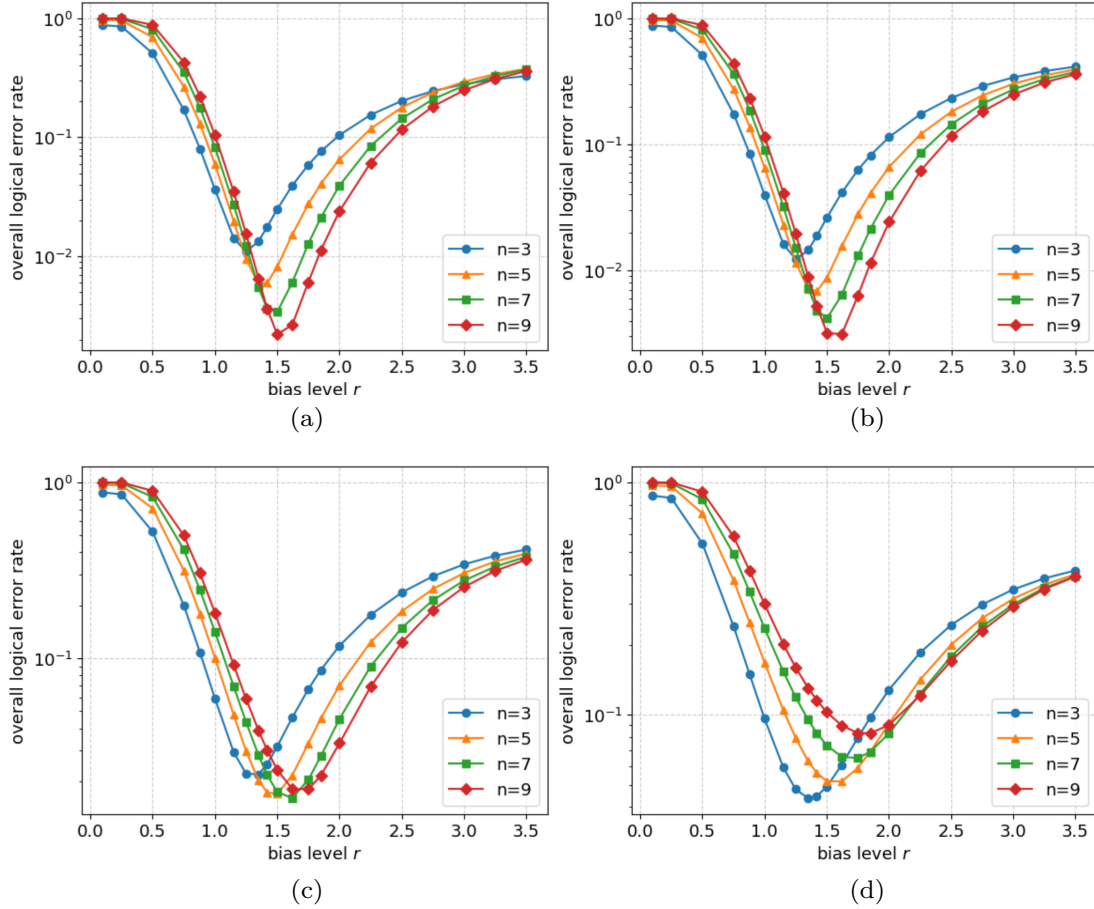


FIG. 16. Relation between the overall logical error rate P_{fail} and bias level r for $\Delta = 0.5$ and (a) $\tilde{\Delta} = 0$, (b) $\tilde{\Delta} = 0.05$, (c) $\tilde{\Delta} = 0.13$, and (d) $\tilde{\Delta} = 0.2$.

The overall logical error rate after the error correction is given by

$$P_{\text{fail}} = 1 - [1 - P_Z(\sqrt{(\Delta/r)^2 + 2\tilde{\Delta}^2})]^{n-1} \times [1 - P_Z(\sqrt{(\Delta/r)^2 + n\tilde{\Delta}^2})][1 - P_{f,n\text{-rep}}(r\Delta, \tilde{\Delta})], \quad (31)$$

where the expression for $P_Z(\Delta)$ is the same as $P_{\tilde{X}}(\Delta)$, which is given by Eq. (15).

The calculation of the exact threshold for $\tilde{\Delta}$ is challenging and we leave it for future work. Here, we provide evidence showing that there exists a nonzero threshold for $\tilde{\Delta}$. The relation between the overall logical error rate P_{fail} and bias level r is shown in Fig. 16 with $\Delta = 0.5$ and $\tilde{\Delta} = 0.0, 0.05, 0.13, 0.2$. We can see that, for every n , the logical error rate has a minimum corresponding to the optimal bias level r_{opt} . When $r < r_{\text{opt}}$, the displacement error from momentum space dominates; while when $r > r_{\text{opt}}$, the displacement error from position space dominates. In addition, the optimal bias level increases when the code size increases. For a sufficiently small $\tilde{\Delta}$, the minimal overall logical error rate decreases as the code size n increases, as shown in Fig. 16(a) with $\tilde{\Delta} = 0$ and in Fig. 16(b) with $\tilde{\Delta} = 0.05$. This implies that for these values of $\tilde{\Delta}$, the concatenation of GKP code with repetition code shows advantages. While for a large $\tilde{\Delta}$,

say, $\tilde{\Delta} = 0.2$, we can see from Fig. 16(d) that the minimal overall logical error rate increases as the code size n increases. As shown in Fig. 16(c) with $\tilde{\Delta} = 0.13$, the minimal overall logical error rate first decreases and then increases as the code size n increases. This implies the threshold of $\tilde{\Delta}$ should be between 0.05 and 0.13. But one should note that, according to the authors of Ref. [40], Δ has a threshold above which the concatenation with repetition code shows no advantages even when $\tilde{\Delta} = 0$. The threshold is estimated to be $0.599 \times \sqrt{2} \approx 0.847$ (note that the variance of error distribution of GKP state in our work is twice of that in Ref. [40]). Therefore, both Δ and $\tilde{\Delta}$ have to be below their thresholds so that the concatenation of the GKP code with the repetition code can show advantages.

The case for $\tilde{\Delta} = 0.13$, which is a slightly smaller than $\tilde{\Delta}_{07} \approx 0.139$ given in Sec. IV B where only error correction in position space is considered, tells us that when we take into account momentum noise, the condition required to exploit the power of code concatenation is more stringent. This is not limited to the special case where $\Delta = 0.5$, but is valid in general, which can be explained qualitatively as follows. The overall logical error rate can be approximated as $P_{\text{fail}} \sim 1 - (1 - P_Z)^n (1 - P_{f,n\text{-rep}})$, where $(1 - P_Z)^n$ decreases exponentially with increasing n . In the regime of $\tilde{\Delta}$ where $P_{f,n\text{-rep}}$ increases with increasing n , P_{fail} becomes higher for a larger code, indicating that concatenation with repetition code shows

no advantages. In the regime of $\tilde{\Delta}$ where $P_{f,n-\text{rep}}$ decreases with increasing n , $P_{f,n-\text{rep}}$ has to decrease fast enough with increasing n , so that the decreasing of $(1 - P_2)^n$ can be compensated and P_{fail} decreases with increasing n . Hence the threshold of $\tilde{\Delta}$ must be lower than the case where only error correction in position space is considered.

For biased noise, concatenating GKP codes with the repetition code significantly reduces the logical error rate. To further suppress the logical error, in particular, to correct the momentum displacement error, one can consider the GKP repetition code as an elementary code block and further concatenate it with other qubit codes. Concatenating the GKP repetition code, which achieves a low logical error rate with low overhead, with other high-level codes could potentially reduce the resource overhead for fault tolerant computation. For the isotropic noise or not highly biased noise, one can either introduce an anisotropic GKP code and concatenate it with repetition code [40], or directly concatenate the GKP code with qubit codes that can correct both bit-flip and phase-flip errors, e.g., the surface code [28–33] or color code [34–36].

VI. CONCLUSION AND OUTLOOKS

We study the concatenation of GKP code with repetition code to correct biased random displacement errors with finite-energy ancillary GKP qubits. The error correction procedure consists of one round of GKP error correction, concatenation with repetition code, syndrome measurement, and recovery operation. The purpose of the GKP error correction is to correct displacement errors before concatenation to alleviate the heavy burden of the repetition code.

We find that there exists a critical value for the noise variance of the ancillary qubits, below which the logical Pauli \tilde{X} error rate decreases as the size of the repetition code increases; and there is a slightly different critical value for the noise variance of the ancillary qubits, above which the logical Pauli \tilde{X} error rate increases as the size of the repetition code increases. These critical values for the noise variance of the ancillary qubits depend on the noise variance of the data qubits, and they increase monotonically as the noise variance of the data qubits increases. Their ratio is lower bounded by 1/16 and upper bounded by 1/4. We also show that the GKP error correction before concatenation with the repetition code is necessary, otherwise the logical Pauli \tilde{X} error rate cannot be reduced even for ideal ancillary GKP qubits.

We then use the GKP repetition code to correct biased noise, for which the random displacement errors in momen-

tum space are assumed to be smaller than that in position space, and therefore, no further concatenation is introduced to correct them. We provide a qualitative analysis showing that there exists a nonvanishing threshold for the noise variance of the ancillary GKP qubit, below which the concatenation with repetition code of larger size can lead to lower overall logical error rate, albeit with a higher level of noise bias. Therefore, the concatenation with the repetition code shows advantages when both $\tilde{\Delta}$ and Δ are below the corresponding thresholds.

Although we take into account the effects of finite-energy ancillary GKP qubits, there are still assumptions needed to be relaxed in future work. For example, quantum operations (SUM gates and recovery operations) are assumed to be ideal, measurement is assumed to be unbiased, and most importantly, the generation of the encoded states of the GKP repetition code is not well studied. Actually, the n input GKP states before encoding are nonideal states, so the degree of squeezing of the n data qubits after encoding are not the same. However, we use an encoded state with equal degree of squeezing only to facilitate calculations, and focus on the relation between performance of the error correction and the quality of the ancillary qubits. Hence, our work only provides a lower limit of the logical error rate of the error correction code. There are some other aspects needed to further explore. It is interesting and important to check whether there is a noninfinite squeezing threshold for the ancillary GKP qubits for an arbitrarily large GKP repetition code. This can be estimated, for example, by using the Monte Carlo simulation. In addition, one needs to consider the finite-energy encoded states that can be efficiently prepared in the experiment, and the envelope-preserving SUM gate.

ACKNOWLEDGMENTS

This work is supported by the Fundamental Research Funds for the Central Universities, HUST (Grant No. 5003012068), and Wuhan Young Talent Research Funds (Grant No. 0106012013).

APPENDIX A: FINITE-ENERGY GKP STATE

By discussing some examples, we can see that the GKP states defined in Eq. (2) are finite-energy. In the first example, we assume $|\tilde{\xi}\rangle = |\tilde{0}\rangle$, then

$$|\tilde{0}\rangle = N_0 \int dudv \eta(u, v) e^{-i\tilde{u}\tilde{p} + i\tilde{v}\tilde{q}} |\tilde{0}\rangle. \quad (\text{A1})$$

Consider the wave function of state $|\tilde{0}\rangle$ in position space

$$\begin{aligned} \tilde{\psi}_0(q) &= \langle q | \tilde{0} \rangle = N_0 \int dudv \eta(u, v) \langle q | e^{-i\tilde{u}\tilde{p} + i\tilde{v}\tilde{q}} |\tilde{0}\rangle = N_0 \sum_{n=-\infty}^{+\infty} \int dudv \eta(u, v) e^{-i\tilde{u}v/2} e^{i\tilde{v}q} \langle q | 2n\sqrt{\pi} + u \rangle_q \\ &= N_0 \sum_{n=-\infty}^{+\infty} \int dv \eta(q - 2n\sqrt{\pi}, v) e^{-i(q-2n\sqrt{\pi})v/2} e^{i\tilde{v}q} = \sqrt{2}N_0 \sqrt{\frac{\kappa}{\Delta}} \sum_{n=-\infty}^{+\infty} e^{-\frac{(q-2n\sqrt{\pi})^2}{2\Delta^2}} e^{-\frac{\kappa^2(q+2n\sqrt{\pi})^2}{8}} \\ &= \sqrt{2}N_0 \sqrt{\frac{\kappa}{\Delta}} \sum_{n=-\infty}^{+\infty} \exp\left\{-\frac{4\pi n^2 \kappa^2}{2(1 + \Delta^2 \kappa^2/4)}\right\} \exp\left\{-\frac{1 + \Delta^2 \kappa^2/4}{2\Delta^2} \left[q - \left(\frac{1 - \Delta^2 \kappa^2/4}{1 + \Delta^2 \kappa^2/4}\right) 2n\sqrt{\pi}\right]^2\right\}. \end{aligned} \quad (\text{A2})$$

It is evident that the wave function $\tilde{\psi}_0(q)$ is a sum of a sequence of Gaussian functions weighted by a function that rapidly decreases when n increases, therefore, the wave function is normalizable and is finite-energy. Note that the spacing between the Gaussian peaks is slightly modified

$$2\sqrt{\pi} \rightarrow 2\sqrt{\pi} \left(\frac{1 - \Delta^2 \kappa^2 / 4}{1 + \Delta^2 \kappa^2 / 4} \right), \quad (\text{A3})$$

and the variance is also slightly changed

$$\Delta^2 \rightarrow \frac{\Delta^2}{1 + \Delta^2 \kappa^2 / 4}. \quad (\text{A4})$$

When both Δ and κ are sufficiently small, the higher-order term $\Delta^2 \kappa^2$ can be neglected, then the wave function $\tilde{\psi}_0(q)$

can be approximated as

$$\begin{aligned} \tilde{\psi}_0(q) &\approx \sqrt{2} N_0 \sqrt{\frac{\kappa}{\Delta}} \sum_{n=-\infty}^{+\infty} e^{-2\pi n^2 \kappa^2} e^{-(q-2n\sqrt{\pi})^2 / 2\Delta^2} \\ &\approx \left(\frac{4\kappa^2}{\pi \Delta^2} \right)^{1/4} \sum_{n=-\infty}^{+\infty} e^{-2\pi n^2 \kappa^2} e^{-(q-2n\sqrt{\pi})^2 / 2\Delta^2}, \end{aligned}$$

where we used the approximation that $N_0^2 \approx 1/\sqrt{\pi}$ when Δ and κ are small.

Then the wave function of state $|\tilde{0}\rangle$ in the momentum space can be calculated in a similar way

$$\begin{aligned} \tilde{\psi}_0(p) &= \langle p | \tilde{0} \rangle = N_0 \int du dv \eta(u, v) \langle p | e^{-iu\hat{p}+iv\hat{q}} | \tilde{0} \rangle = N_0 \sum_{n=-\infty}^{+\infty} \int du dv \eta(u, v) e^{iuv/2} e^{-iup} \langle p | n\sqrt{\pi} + v \rangle_p \\ &= N_0 \sum_{n=-\infty}^{+\infty} \int dv \eta(u, p - n\sqrt{\pi}) e^{i(p-n\sqrt{\pi})u/2} e^{-iup} = \sqrt{2} N_0 \sqrt{\frac{\Delta}{\kappa}} \sum_{n=-\infty}^{+\infty} e^{-\frac{(p-n\sqrt{\pi})^2}{2\kappa^2}} e^{-\frac{\Delta^2(p+n\sqrt{\pi})^2}{8}} \\ &= \sqrt{2} N_0 \sqrt{\frac{\Delta}{\kappa}} \sum_{n=-\infty}^{+\infty} \exp \left\{ -\frac{\pi n^2 \Delta^2}{2(1 + \Delta^2 \kappa^2 / 4)} \right\} \exp \left\{ -\frac{1 + \Delta^2 \kappa^2 / 4}{2\kappa^2} \left[p - \left(\frac{1 - \Delta^2 \kappa^2 / 4}{1 + \Delta^2 \kappa^2 / 4} \right) n\sqrt{\pi} \right]^2 \right\}. \quad (\text{A5}) \end{aligned}$$

Note that the spacing between the Gaussian peaks is slightly modified

$$\sqrt{\pi} \rightarrow \sqrt{\pi} \left(\frac{1 - \Delta^2 \kappa^2 / 4}{1 + \Delta^2 \kappa^2 / 4} \right), \quad (\text{A6})$$

and the variance is also slightly changed

$$\kappa^2 \rightarrow \frac{\kappa^2}{1 + \Delta^2 \kappa^2 / 4}. \quad (\text{A7})$$

When both Δ and κ are small, the higher-order term $\Delta^2 \kappa^2$ can be neglected, then the wave function $\tilde{\psi}_0(p)$ can be approximated as

$$\tilde{\psi}_0(p) \approx \left(\frac{4\Delta^2}{\pi \kappa^2} \right)^{1/4} \sum_{n=-\infty}^{+\infty} e^{-\pi n^2 \Delta^2 / 2} e^{-(p-n\sqrt{\pi})^2 / 2\kappa^2}. \quad (\text{A8})$$

In the second example, we consider $|\tilde{\xi}\rangle = |\tilde{1}\rangle$, then

$$|\tilde{1}\rangle = N_1 \int du dv \eta(u, v) e^{-iu\hat{p}+iv\hat{q}} |\tilde{1}\rangle. \quad (\text{A9})$$

Using the expression of $|\tilde{1}\rangle = \sum_n |(2n+1)\sqrt{\pi}\rangle_q$ in position space, we can similarly derive its wave function

$$\begin{aligned} \tilde{\psi}_1(q) &= \langle q | \tilde{1} \rangle = N_1 \int du dv \eta(u, v) \langle q | e^{-iu\hat{p}+iv\hat{q}} | \tilde{1} \rangle = \sqrt{2} N_1 \sqrt{\frac{\kappa}{\Delta}} \sum_{n=-\infty}^{+\infty} e^{-\frac{[q-(2n+1)\sqrt{\pi}]^2}{2\Delta^2}} e^{-\frac{\kappa^2[q+(2n+1)\sqrt{\pi}]^2}{8}} \\ &= \sqrt{2} N_1 \sqrt{\frac{\kappa}{\Delta}} \sum_{n=-\infty}^{+\infty} \exp \left\{ -\frac{\pi(2n+1)^2 \kappa^2}{2(1 + \Delta^2 \kappa^2 / 4)} \right\} \exp \left\{ -\frac{1 + \Delta^2 \kappa^2 / 4}{2\Delta^2} \left[q - \left(\frac{1 - \Delta^2 \kappa^2 / 4}{1 + \Delta^2 \kappa^2 / 4} \right) (2n+1)\sqrt{\pi} \right]^2 \right\}. \quad (\text{A10}) \end{aligned}$$

When both Δ and κ are sufficiently small, the higher-order term $\Delta^2 \kappa^2$ can be neglected, then the wave function $\tilde{\psi}_1(q)$ can be approximated as

$$\tilde{\psi}_1(q) \approx \sqrt{2} N_1 \sqrt{\frac{\kappa}{\Delta}} \sum_{n=-\infty}^{+\infty} e^{-\frac{(2n+1)^2 \pi \kappa^2}{2}} e^{-\frac{[q-(2n+1)\sqrt{\pi}]^2}{2\Delta^2}} \approx \left(\frac{4\kappa^2}{\pi \Delta^2} \right)^{1/4} \sum_{n=-\infty}^{+\infty} e^{-\frac{(2n+1)^2 \pi \kappa^2}{2}} e^{-\frac{[q-(2n+1)\sqrt{\pi}]^2}{2\Delta^2}}, \quad (\text{A11})$$

where we use the approximation that $N_1^2 \approx 1/\sqrt{\pi}$ when Δ and κ are small.

The wave function in momentum space can be calculated in a similar way,

$$\begin{aligned}\tilde{\psi}_1(p) &= \langle p | \tilde{0} \rangle = N_1 \int dudv \eta(u, v) \langle p | e^{-iu\hat{p}+iv\hat{q}} | \tilde{1} \rangle = \sqrt{2}N_1 \sqrt{\frac{\Delta}{\kappa}} \sum_{n=-\infty}^{+\infty} (-1)^n e^{-\frac{(p-n\sqrt{\pi})^2}{2\kappa^2}} e^{-\frac{\Delta^2(p+n\sqrt{\pi})^2}{8}} \\ &= \sqrt{2}N_1 \sqrt{\frac{\Delta}{\kappa}} \sum_{n=-\infty}^{+\infty} (-1)^n \exp \left\{ -\frac{\pi n^2 \Delta^2}{2(1 + \Delta^2 \kappa^2/4)} \right\} \exp \left\{ -\frac{1 + \Delta^2 \kappa^2/4}{2\kappa^2} \left[p - \left(\frac{1 - \Delta^2 \kappa^2/4}{1 + \Delta^2 \kappa^2/4} \right) n\sqrt{\pi} \right]^2 \right\}.\end{aligned}\quad (\text{A12})$$

When both Δ and κ are small, the higher-order term $\Delta^2 \kappa^2$ can be neglected, then the wave function $\tilde{\psi}_1(p)$ can be approximated as

$$\tilde{\psi}_1(p) \approx \left(\frac{4\Delta^2}{\pi\kappa^2} \right)^{1/4} \sum_{n=-\infty}^{+\infty} (-1)^n e^{-\pi n^2 \Delta^2/2} e^{-(p-n\sqrt{\pi})^2/2\kappa^2}.\quad (\text{A13})$$

According to the definition of the Wigner function and the expression for $\tilde{\psi}_0(q)$, it is straightforward to calculate the Wigner function of the finite-energy GKP state $|\tilde{0}\rangle$,

$$\begin{aligned}W(q, p; |\tilde{0}\rangle \langle \tilde{0}|) &= \sqrt{\pi}N_0^2 \sum_{m,n} e^{-\pi\Delta_s^2 m^2/4 - 4\pi\kappa_s^2 n^2} \exp \left\{ -\frac{(p - m\sqrt{\pi}\gamma/2)^2}{\kappa_s^2} - \frac{(q - 2n\sqrt{\pi}\gamma)^2}{\Delta_s^2} \right\} \\ &+ \sqrt{\pi}N_0^2 \sum_{m,n} (-1)^m e^{-\pi\Delta_s^2 m^2/4 - \pi\kappa_s^2 (2n+1)^2} \exp \left\{ -\frac{(p - m\sqrt{\pi}\gamma/2)^2}{\kappa_s^2} - \frac{[q - (2n+1)\sqrt{\pi}\gamma]^2}{\Delta_s^2} \right\},\end{aligned}\quad (\text{A14})$$

where $\Delta_s = \Delta/\sqrt{1 + \Delta^2 \kappa^2/4}$, $\kappa_s = \kappa/\sqrt{1 + \Delta^2 \kappa^2/4}$ and $\gamma = \frac{1 - \Delta^2 \kappa^2/4}{1 + \Delta^2 \kappa^2/4}$. When both Δ and κ are sufficiently small, the higher-order term $\Delta^2 \kappa^2$ can be neglected, namely, $\Delta_s \rightarrow \Delta$, $\kappa_s \rightarrow \kappa$, and $\gamma \rightarrow 1$. The Wigner function of the finite-energy GKP state can be approximated as

$$\begin{aligned}W(q, p; |\tilde{0}\rangle \langle \tilde{0}|) &\approx \sum_{m,n} e^{-\pi\Delta^2 m^2/4 - 4\pi\kappa^2 n^2} \exp \left\{ -\frac{(p - m\sqrt{\pi}/2)^2}{\kappa^2} - \frac{(q - 2n\sqrt{\pi})^2}{\Delta^2} \right\} \\ &+ \sum_{m,n} (-1)^m e^{-\pi\Delta^2 m^2/4 - \pi\kappa^2 (2n+1)^2} \exp \left\{ -\frac{(p - m\sqrt{\pi}/2)^2}{\kappa^2} - \frac{[q - (2n+1)\sqrt{\pi}]^2}{\Delta^2} \right\}.\end{aligned}\quad (\text{A15})$$

Consider the Wigner function of the ideal GKP state $|\tilde{0}\rangle$ after going through a GDC. The density matrix is

$$\hat{\rho} = \int dudv f(u, v) \hat{D}(u, v) |\tilde{0}\rangle \langle \tilde{0}| \hat{D}^\dagger(u, v) = \sum_{n,m} \int dudv f(u, v) e^{2i\sqrt{\pi}v(n-m)} |2n\sqrt{\pi} + u\rangle_q \langle 2m\sqrt{\pi} + u|.\quad (\text{A16})$$

then the Wigner function can be calculated as

$$\begin{aligned}W(q, p; \hat{\rho}) &= \frac{1}{4\pi\sqrt{\pi}\Delta\kappa} \sum_{m,n} \exp \left\{ -\frac{(p - m\sqrt{\pi}/2)^2}{\delta_p^2} - \frac{(q - 2n\sqrt{\pi})^2}{\delta_q^2} \right\} \\ &+ \frac{1}{4\pi\sqrt{\pi}\Delta\kappa} \sum_{m,n} (-1)^m \exp \left\{ -\frac{(p - m\sqrt{\pi}/2)^2}{\delta_p^2} - \frac{[q - (2n+1)\sqrt{\pi}]^2}{\delta_q^2} \right\}.\end{aligned}\quad (\text{A17})$$

After the action of GDC, the new Wigner function $W(q, p)$ is related to the old Wigner function $W_0(q, p)$ via

$$W(q, p) = \int dudv f(u, v) W_0(q + u, p + v) = \int dudv f(u - q, v - p) W_0(u, v),\quad (\text{A18})$$

which implies that the new Wigner function is the convolution of the old Wigner function and the noise distribution function f . Although the finite-energy GKP state is not Gaussian, their Wigner function can be written as a sum of a sequence of Gaussian functions. Since the convolution of two Gaussian functions gives also a Gaussian function, the Wigner function of a finite-energy GKP state after going through a GDC is still a sum of a sequence of Gaussian functions. Furthermore, the variances of the new Gaussian functions are the sum of the variances of the old Gaussian functions and those of noise distribution function. Suppose $W_0(q, p) = W(q, p; |\tilde{0}\rangle \langle \tilde{0}|)$, then the Wigner function after going through the GDC is given

by

$$W_{\text{GDC}}(q, p; |\tilde{0}\rangle \langle \tilde{0}|) \approx \frac{\Delta\kappa}{\sqrt{(\delta_q^2 + \Delta^2)(\delta_p^2 + \kappa^2)}} \left\{ \sum_{m,n} e^{-\pi\Delta^2 m^2/4 - 4\pi\kappa^2 n^2} \exp\left[-\frac{(p - m\sqrt{\pi}/2)^2}{\kappa^2 + \delta_p^2} - \frac{(q - 2n\sqrt{\pi})^2}{\Delta^2 + \delta_q^2}\right] \right. \\ \left. + \sum_{m,n} (-1)^m e^{-\pi\Delta^2 m^2/4 - \pi\kappa^2(2n+1)^2} \exp\left[-\frac{(p - m\sqrt{\pi}/2)^2}{\kappa^2 + \delta_p^2} - \frac{(q - (2n+1)\sqrt{\pi})^2}{\Delta^2 + \delta_q^2}\right] \right\}. \quad (\text{A19})$$

APPENDIX B: ERROR DISTRIBUTION OF GKP STATE AFTER SUM GATE WITH FINITE-ENERGY ANCILLARY QUBIT

We give the detailed calculation of the error distribution of GKP state after GKP error correction with a finite-energy ancillary qubit, i.e., we calculate the probability distribution of the variable u' given by Eq. (18), with the probability distribution of u_1 and u_2 given by Eq. (16). We first need to calculate the probability $P(u' \leq x)$ for a given x ,

$$P(u' \leq x) = \sum_k P\left[u_2 \geq k\sqrt{\pi} - x \text{ and } \left(k - \frac{1}{2}\right)\sqrt{\pi} \leq u_1 + u_2 < \left(k + \frac{1}{2}\right)\sqrt{\pi}\right] \\ = \sum_k \int_{k\sqrt{\pi}-x}^{+\infty} f_{q_2}(u_2) du_2 \int_{(k-1/2)\sqrt{\pi}-u_2}^{(k+1/2)\sqrt{\pi}-u_2} f_{q_1}(u_1) du_1 \\ = \frac{1}{2} \sum_k \int_{k\sqrt{\pi}-x}^{+\infty} du_2 f_{q_2}(u_2) \\ \times \left[\text{erf}\left(\frac{(k+1/2)\sqrt{\pi} - u_2}{\Delta}\right) - \text{erf}\left(\frac{(k-1/2)\sqrt{\pi} - u_2}{\Delta}\right) \right]. \quad (\text{B1})$$

Then the probability distribution of u' is obtained by taking derivative with respect to x ,

$$F(u' = x) = \frac{dP(u' \leq x)}{dx} \\ = \frac{1}{2} \sum_k f_{q_2}(u_2 = k\sqrt{\pi} - x) \left[\text{erf}\left(\frac{\sqrt{\pi}/2 + x}{\Delta}\right) - \text{erf}\left(\frac{-\sqrt{\pi}/2 + x}{\Delta}\right) \right] \\ = \frac{1}{2\sqrt{\pi}\tilde{\Delta}} \left[\text{erf}\left(\frac{\sqrt{\pi}/2 + x}{\Delta}\right) - \text{erf}\left(\frac{-\sqrt{\pi}/2 + x}{\Delta}\right) \right] \\ \sum_t \exp\left[-\frac{(x - t\sqrt{\pi})^2}{\tilde{\Delta}^2}\right]. \quad (\text{B2})$$

Finally Eq. (19) is obtained by simply rewriting the above result.

APPENDIX C: CLASSICAL n -QUBIT BIT-FLIP REPETITION CODE

In the n -qubit bit-flip repetition code [47,48], n physical qubits are introduced to encode one logical qubit, in particular, the single-qubit state $\alpha|0\rangle + \beta|1\rangle$ is encoded as follows:

$$|\psi\rangle = \alpha|0\rangle + \beta|1\rangle \rightarrow |\bar{\psi}\rangle = \alpha|00\dots 0\rangle + \beta|11\dots 1\rangle. \quad (\text{C1})$$

If one of these n qubits was flipped, the flipped qubit can be detected by comparing any two of these n qubits and then applying the majority rule, which is known as the syndrome measurement. Once the flipped qubit is identified, it can be corrected by applying a Pauli X operator. The n -qubit repetition code is able to correct any m -qubit bit-flip error, with $1 \leq m \leq (n-1)/2$. Denote the bit-flip error rate of a single physical qubit as p , then the failure probability of the n -qubit repetition code is given by

$$P_{f,n\text{-rep}}^{\text{class}} = \sum_{i=(n+1)/2}^n C_n^i p^i (1-p)^{n-i}. \quad (\text{C2})$$

To realize the comparison between physical qubits without collapsing the encoded state, one needs to introduce ancillary qubits to perform the syndrome measurement. There are $C_n^0 + C_n^1 + \dots + C_n^{(n-1)/2} = 2^{n-1}$ possibilities that up to $(n-1)/2$ qubits are flipped, i.e., 2^{n-1} correctable errors. Therefore, 2^{n-1} syndromes are needed to decode these errors, which implies $(n-1)$ ancillary GKP qubits are required to perform syndrome measurement. The comparison of states of two qubits is implemented by the CNOT gate.

The qubit with bit-flip error is identified through the measurement outcome of the ancillary qubits, known as the syndrome. Take the simplest three-qubit repetition code as an example, the one-to-one correspondence between the syndrome and the single-qubit bit-flip error of classical three-qubit repetition code [47,48] is summarized in Table III. As an example, if the ancillary qubit A'_1 is flipped while A'_2 is not, then the states of the data qubits D_1 and D_2 are different, while the states of the data qubits D_1 and D_3 are the same. This implies that the data qubit D_2 is flipped.

TABLE III. Correspondence between syndromes and single-qubit bit-flip errors for the classical three-qubit repetition code.

Syndrome	Final state	Error
0 0	$\alpha 000\rangle + \beta 111\rangle$	No error
1 1	$\alpha 100\rangle + \beta 011\rangle$	Bit flip on data qubit 1
1 0	$\alpha 010\rangle + \beta 101\rangle$	Bit flip on data qubit 2
0 1	$\alpha 001\rangle + \beta 110\rangle$	Bit flip on data qubit 3

APPENDIX D: CALCULATION OF THE FAILURE PROBABILITY OF THREE-QUBIT GKP REPETITION CODE

The correspondence between measurement outcomes and the logical Pauli \bar{X} error on different GKP qubits of three-qubit GKP repetition code is summarized in Table I. However, this decoding procedure may result in misidentification of the error, which is different from that of the classical three-qubit repetition code. To calculate the failure probability of three-qubit GKP repetition code, we need to reverse the decoding process and impose some conditions to be satisfied instead. For example, if no error occurs, we need $M_1 \in \text{NPZ}$ and $M_2 \in \text{NPZ}$ to give the correct identification, and the area outside $M_1 \in \text{NPZ}$ and $M_2 \in \text{NPZ}$ must lead to failure. Similar rules apply for other cases. All possible circumstances are summarized as follows:

- (1) Case 1: If no error occurs \Rightarrow we require $M_1 \in \text{NPZ}, M_2 \in \text{NPZ}$;
- (2) Case 2: If \bar{X} applies on data qubit $D_1 \Rightarrow$ we require $M_1 \in \text{PZ}, M_2 \in \text{PZ}$;
- (3) Case 3: If \bar{X} applies on data qubit $D_2 \Rightarrow$ we require $M_1 \in \text{PZ}, M_2 \in \text{NPZ}$;
- (4) Case 4: If \bar{X} applies on data qubit $D_3 \Rightarrow$ we require $M_1 \in \text{NPZ}, M_2 \in \text{PZ}$;
- (5) Case 5: If errors occur on more than one data qubit, with probability $3P_F^2(1 - P_F) + P_F^3 \Rightarrow$ error correction fails.

Now we calculate the failure probability for the above five cases, the sum of which gives the total failure probability. Consider case 1, there are five constraints needed to be satisfied simultaneously,

$$\begin{aligned} \text{No Pauli } \bar{X} \text{ error} &\Rightarrow |u'_1 - 2m_1\sqrt{\pi}| < \frac{\sqrt{\pi}}{2}, |u'_2 - 2m_2\sqrt{\pi}| < \frac{\sqrt{\pi}}{2}, |u'_3 - 2m_3\sqrt{\pi}| < \frac{\sqrt{\pi}}{2}, \\ M_1 \in \text{NPZ}, M_2 \in \text{NPZ} &\Rightarrow |u'_1 + u'_2 + \alpha_1 - 2n_1\sqrt{\pi}| < \frac{\sqrt{\pi}}{2}, |u'_1 + u'_3 + \alpha_2 - 2n_2\sqrt{\pi}| < \frac{\sqrt{\pi}}{2}, \end{aligned} \quad (\text{D1})$$

where $m_i \in \mathbb{Z}$ and $n_i \in \mathbb{Z}$. The probability of success is obtained by integrating the probability distribution of five variables in the domain defined by these five inequalities. However, it is challenging to derive an analytic expression for the success probability, which requires a five-dimensional linear programming. Therefore, a numerical integration method is used instead, which proceeds in two steps. We first fix a point (u'_1, u'_2, u'_3) in the domain defined by the first three inequalities in Eq. (D1), then the success probability at this given point is

$$\begin{aligned} P_\alpha^1(u'_1, u'_2, u'_3) &= \left(\sum_{n_1} \int_{-\sqrt{\pi}/2+2n_1\sqrt{\pi}-u'_1-u'_2}^{\sqrt{\pi}/2+2n_1\sqrt{\pi}-u'_1-u'_2} f_{q'_1}(\alpha_1) d\alpha_1 \right) \left(\sum_{n_2} \int_{-\sqrt{\pi}/2+2n_2\sqrt{\pi}-u'_1-u'_3}^{\sqrt{\pi}/2+2n_2\sqrt{\pi}-u'_1-u'_3} f_{q'_2}(\alpha_2) d\alpha_2 \right) \\ &\approx \frac{1}{4} \left[\text{erf} \left(\frac{\frac{\sqrt{\pi}}{2} - u'_1 - u'_2}{\bar{\Delta}} \right) - \text{erf} \left(\frac{-\frac{\sqrt{\pi}}{2} - u'_1 - u'_2}{\bar{\Delta}} \right) \right] \left[\text{erf} \left(\frac{\frac{\sqrt{\pi}}{2} - u'_1 - u'_3}{\bar{\Delta}} \right) - \text{erf} \left(\frac{-\frac{\sqrt{\pi}}{2} - u'_1 - u'_3}{\bar{\Delta}} \right) \right], \end{aligned} \quad (\text{D2})$$

where we have only kept one term with $n_1 = n_2 = 0$ in the summation because the contribution from other terms is negligible. Then the failure probability of case 1 is given by integrating the failure probability $1 - P_\alpha^1(u'_1, u'_2, u'_3)$ over all points satisfying the first three constraints in Eq. (D1), weighted by the probability distribution $F(u'_1, u'_2, u'_3) = F(u'_1)F(u'_2)F(u'_3)$,

$$\begin{aligned} P_{f,3\text{-rep}}^1 &= \int_{u'_1 \in \text{NPZ}} \int_{u'_2 \in \text{NPZ}} \int_{u'_3 \in \text{NPZ}} F(u'_1, u'_2, u'_3) [1 - P_\alpha^1(u'_1, u'_2, u'_3)] du'_1 du'_2 du'_3 \\ &\approx \int_{u'_1 = -\sqrt{\pi}/2}^{\sqrt{\pi}/2} \int_{u'_2 = -\sqrt{\pi}/2}^{\sqrt{\pi}/2} \int_{u'_3 = -\sqrt{\pi}/2}^{\sqrt{\pi}/2} F(u'_1, u'_2, u'_3) [1 - P_\alpha^1(u'_1, u'_2, u'_3)] du'_1 du'_2 du'_3, \end{aligned} \quad (\text{D3})$$

where we only kept one term with $m_1 = m_2 = m_3 = 0$ in the summation because the contribution from other terms is negligible.

In a similar way, we can derive the failure probability for case 2 by taking into account the condition that $u'_1 \in \text{PZ}, u'_2 \in \text{NPZ}$ and $u'_3 \in \text{NPZ}$,

$$\begin{aligned} P_{f,3\text{-rep}}^2 &= \int_{u'_1 \in \text{PZ}} \int_{u'_2 \in \text{NPZ}} \int_{u'_3 \in \text{NPZ}} F(u'_1, u'_2, u'_3) [1 - P_\alpha^2(u'_1, u'_2, u'_3)] du'_1 du'_2 du'_3 \\ &\approx 2 \int_{u'_1 = \sqrt{\pi}/2}^{3\sqrt{\pi}/2} \int_{u'_2 = -\sqrt{\pi}/2}^{\sqrt{\pi}/2} \int_{u'_3 = -\sqrt{\pi}/2}^{\sqrt{\pi}/2} F(u'_1, u'_2, u'_3) [1 - P_\alpha^2(u'_1, u'_2, u'_3)] du'_1 du'_2 du'_3, \end{aligned} \quad (\text{D4})$$

where $P_\alpha^2(u'_1, u'_2, u'_3)$ is the success probability for a given point (u'_1, u'_2, u'_3) when $M_1 \in \text{PZ}$ and $M_2 \in \text{PZ}$,

$$\begin{aligned} P_\alpha^2(u'_1, u'_2, u'_3) &= \left(\sum_{n_1} \int_{\sqrt{\pi}/2+2n_1\sqrt{\pi}-u'_1-u'_2}^{3\sqrt{\pi}/2+2n_1\sqrt{\pi}-u'_1-u'_2} f_{q'_1}(\alpha_1) d\alpha_1 \right) \left(\sum_{n_2} \int_{\sqrt{\pi}/2+2n_2\sqrt{\pi}-u'_1-u'_3}^{3\sqrt{\pi}/2+2n_2\sqrt{\pi}-u'_1-u'_3} f_{q'_2}(\alpha_2) d\alpha_2 \right) \\ &\approx \frac{1}{4} \left[\text{erf} \left(\frac{\frac{3\sqrt{\pi}}{2} - u'_1 - u'_2}{\bar{\Delta}} \right) - \text{erf} \left(\frac{\frac{\sqrt{\pi}}{2} - u'_1 - u'_2}{\bar{\Delta}} \right) \right] \left[\text{erf} \left(\frac{\frac{3\sqrt{\pi}}{2} - u'_1 - u'_3}{\bar{\Delta}} \right) - \text{erf} \left(\frac{\frac{\sqrt{\pi}}{2} - u'_1 - u'_3}{\bar{\Delta}} \right) \right]. \end{aligned} \quad (\text{D5})$$

$P_\alpha^3(u'_1, u'_2, u'_3)$ and $P_\alpha^4(u'_1, u'_2, u'_3)$ can also be calculated by the similar way, and it can be shown that the failure probabilities of cases 3 and 4 are the same as that of the case 2, namely,

$$P_{f,3\text{-rep}}^2 = P_{f,3\text{-rep}}^3 = P_{f,3\text{-rep}}^4. \quad (\text{D6})$$

The failure probability of case 5 is

$$P_{f,3\text{-rep}}^5 = 3P_F^2(1 - P_F) + P_F^3. \quad (\text{D7})$$

Finally, the total failure probability of the three-qubit GKP repetition code is

$$\begin{aligned} P_{f,3\text{-rep}}(\Delta, \tilde{\Delta}) &= P_{f,3\text{-rep}}^1 + P_{f,3\text{-rep}}^2 + P_{f,3\text{-rep}}^3 + P_{f,3\text{-rep}}^4 + P_{f,3\text{-rep}}^5 \\ &\approx \int_{u'_1=-\sqrt{\pi}/2}^{\sqrt{\pi}/2} \int_{u'_2=-\sqrt{\pi}/2}^{\sqrt{\pi}/2} \int_{u'_3=-\sqrt{\pi}/2}^{\sqrt{\pi}/2} F(u'_1, u'_2, u'_3) [1 - P_\alpha^1(u'_1, u'_2, u'_3)] du'_1 du'_2 du'_3 \\ &\quad + 6 \int_{u'_1=-\sqrt{\pi}/2}^{3\sqrt{\pi}/2} \int_{u'_2=-\sqrt{\pi}/2}^{\sqrt{\pi}/2} \int_{u'_3=-\sqrt{\pi}/2}^{\sqrt{\pi}/2} F(u'_1, u'_2, u'_3) [1 - P_\alpha^2(u'_1, u'_2, u'_3)] du'_1 du'_2 du'_3 + 3P_F^2(1 - P_F) + P_F^3. \end{aligned} \quad (\text{D8})$$

APPENDIX E: CALCULATION OF THE FAILURE PROBABILITY OF n -QUBIT GKP REPETITION CODE

The correspondence between measurement outcomes and correctable errors of GKP n -qubit repetition code is given by Table II. In the same way as we discuss in the three-qubit GKP repetition code, this decoding procedure may result in misidentification of the error, which is different from that of the classical n -qubit repetition code. Here we provide the detailed calculation of the failure probability of n -qubit GKP repetition code. Similar to the discussion in Appendix D, we need to reverse the decoding process and impose some conditions to be satisfied. All possible cases are summarized as follows:

- (1) Case 1: If no error occurs \Rightarrow we require $M_1, M_2, \dots, M_{n-1} \in \text{NPZ}$;
- (2) Case 2: If \bar{X} applies on data qubit $D_1 \Rightarrow$ we require $M_1, M_2, \dots, M_{n-1} \in \text{PZ}$. We find that this failure probability is the same as all C_n^1 cases where \bar{X} applies on a single data qubit;
- (3) Case i ($3 \leq i \leq \frac{n+1}{2}$): If \bar{X} applies on data qubit $D_1, D_2, \dots, D_{i-1} \Rightarrow$ we require $M_1, \dots, M_{i-2} \in \text{NPZ}, M_{i-1}, \dots, M_{n-1} \in \text{PZ}$. This failure probability is the same as all C_n^{i-1} cases where \bar{X} applies on $i-1$ data qubits;
- (4) Case $\frac{n+3}{2}$: If errors occur on more than $(n-1)/2$ data qubits, with probability $\sum_{j=\frac{n+1}{2}}^n C_n^j P_F^j (1 - P_F)^{n-j} \Rightarrow$ the error correction fails.

Note that we incorporate all C_n^s possibilities where errors occur on s data qubits into one case, and we consider a representative where errors occur on the first s data qubits D_1, D_2, \dots, D_s , for all possibilities have the same failure probability.

Now we calculate the failure probability for these $(n+3)/2$ cases, the sum of which gives the total probability of failure. Consider case 1, there are $2n-1$ constraints needed to be satisfied simultaneously,

$$\begin{aligned} \text{No Pauli } \bar{X} \text{ error} &\Rightarrow |u'_1 - 2s_1\sqrt{\pi}| < \frac{\sqrt{\pi}}{2}, |u'_2 - 2s_2\sqrt{\pi}| < \frac{\sqrt{\pi}}{2}, \dots, |u'_n - 2s_n\sqrt{\pi}| < \frac{\sqrt{\pi}}{2}, \\ M_1, M_2, \dots, M_{n-1} \in \text{NPZ} &\Rightarrow |u'_1 + u'_2 + \alpha_1 - 2t_1\sqrt{\pi}| < \frac{\sqrt{\pi}}{2}, \dots, |u'_1 + u'_n + \alpha_{n-1} - 2t_{n-1}\sqrt{\pi}| < \frac{\sqrt{\pi}}{2}, \end{aligned} \quad (\text{E1})$$

where $s_i \in \mathbb{Z}$ and $t_i \in \mathbb{Z}$. The probability of success is obtained by integrating the probability distribution of $2n-1$ variables in the domain defined by these $2n-1$ inequalities. Similar to the discussion in Sec. IV A, we use the numerical method to calculate the integration. We first fix a point $(u'_1, u'_2, \dots, u'_n)$ defined by the first n inequalities in Eq. (E1), then the success probability at this given point is

$$\begin{aligned} P_\alpha^1(u'_1, \dots, u'_n) &= \left(\sum_{t_1} \int_{-\sqrt{\pi}/2+2t_1\sqrt{\pi}-u'_1-u'_2}^{\sqrt{\pi}/2+2t_1\sqrt{\pi}-u'_1-u'_2} f_{q'_1}(\alpha_1) d\alpha_1 \right) \times \dots \times \left(\sum_{t_{n-1}} \int_{-\sqrt{\pi}/2+2t_{n-1}\sqrt{\pi}-u'_1-u'_n}^{\sqrt{\pi}/2+2t_{n-1}\sqrt{\pi}-u'_1-u'_n} f_{q'_{n-1}}(\alpha_{n-1}) d\alpha_{n-1} \right) \\ &\approx \frac{1}{2^{n-1}} \prod_{k=2}^n \left[\text{erf} \left(\frac{\sqrt{\pi}/2 - u'_1 - u'_k}{\tilde{\Delta}} \right) - \text{erf} \left(\frac{-\sqrt{\pi}/2 - u'_1 - u'_k}{\tilde{\Delta}} \right) \right], \end{aligned} \quad (\text{E2})$$

where we only keep one term $t_1 = t_2 = \dots = t_{n-1} = 0$ in the summation because the contribution from other terms is negligible. Then the failure probability of case 1 is given by integrating the failure probability $1 - P_\alpha^1(u'_1, \dots, u'_n)$ over all points satisfying

the constraints in Eq. (E1), weighted by the probability distribution $\prod_{i=1}^n F(u'_i)$,

$$\begin{aligned} P_{f,n\text{-rep}}^1 &= \int_{u'_1 \in \text{NPZ}} \cdots \int_{u'_n \in \text{NPZ}} \left[\prod_{i=1}^n F(u'_i) \right] [1 - P_\alpha^1(u'_1, \dots, u'_n)] du'_1 \cdots du'_n \\ &\approx \int_{u'_1 = -\sqrt{\pi}/2}^{\sqrt{\pi}/2} \cdots \int_{u'_n = -\sqrt{\pi}/2}^{\sqrt{\pi}/2} \left[\prod_{i=1}^n F(u'_i) \right] [1 - P_\alpha^1(u'_1, \dots, u'_n)] du'_1 \cdots du'_n, \end{aligned} \quad (\text{E3})$$

where we only keep one term with $s_1 = s_2 = \cdots = s_n = 0$ in the summation because the contribution from other terms is negligible.

Similarly, we can derive the failure probability of case 2 by taking into account the condition that $u'_1 \in \text{PZ}, u'_2 \in \text{NPZ}, \dots, u'_n \in \text{NPZ}$,

$$\begin{aligned} P_{f,n\text{-rep}}^2 &= \int_{u'_1 \in \text{PZ}} \int_{u'_2 \in \text{NPZ}} \cdots \int_{u'_n \in \text{NPZ}} \left[\prod_{i=1}^n F(u'_i) \right] [1 - P_\alpha^2(u'_1, \dots, u'_n)] du'_1 \cdots du'_n \\ &\approx 2 \int_{u'_1 = \sqrt{\pi}/2}^{3\sqrt{\pi}/2} \int_{u'_2 = -\sqrt{\pi}/2}^{\sqrt{\pi}/2} \cdots \int_{u'_n = -\sqrt{\pi}/2}^{\sqrt{\pi}/2} \left[\prod_{i=1}^n F(u'_i) \right] [1 - P_\alpha^2(u'_1, \dots, u'_n)] du'_1 \cdots du'_n, \end{aligned} \quad (\text{E4})$$

where $P_\alpha^2(u'_1, \dots, u'_n)$ is the success probability for a given point $(u'_1, u'_2, \dots, u'_n)$ when $M_1, M_2, \dots, M_{n-1} \in \text{PZ}$,

$$\begin{aligned} P_\alpha^2(u'_1, \dots, u'_n) &= \left(\sum_{\alpha_1} \int_{\sqrt{\pi}/2 + 2t_1\sqrt{\pi} - u'_1 - u'_2}^{3\sqrt{\pi}/2 + 2t_1\sqrt{\pi} - u'_1 - u'_2} f_{q_1}(\alpha_1) d\alpha_1 \right) \times \cdots \times \left(\sum_{\alpha_{n-1}} \int_{\sqrt{\pi}/2 + 2t_{n-1}\sqrt{\pi} - u'_1 - u'_n}^{3\sqrt{\pi}/2 + 2t_{n-1}\sqrt{\pi} - u'_1 - u'_n} f_{q_{n-1}}(\alpha_{n-1}) d\alpha_{n-1} \right) \\ &\approx \frac{1}{2^{n-1}} \prod_{k=2}^n \left[\text{erf} \left(\frac{3\sqrt{\pi}/2 - u'_1 - u'_k}{\tilde{\Delta}} \right) - \text{erf} \left(\frac{\sqrt{\pi}/2 - u'_1 - u'_k}{\tilde{\Delta}} \right) \right]. \end{aligned} \quad (\text{E5})$$

Note that there are C_n^1 cases giving the same result as case 2, so we need to plus $P_{f,n\text{-rep}}^2$ with C_n^1 in the total failure probability.

In a similar way, the failure probability of case i ($3 \leq i \leq \frac{n+1}{2}$) is given by taking into account the condition that $u'_1, \dots, u'_{i-1} \in \text{PZ}, u'_i, \dots, u'_n \in \text{NPZ}$,

$$\begin{aligned} P_{f,n\text{-rep}}^i &= \int_{u'_1 \in \text{PZ}} \cdots \int_{u'_{i-1} \in \text{PZ}} \int_{u'_i \in \text{NPZ}} \cdots \int_{u'_n \in \text{NPZ}} \left[\prod_{i=1}^n F(u'_i) \right] [1 - P_\alpha^i(u'_1, \dots, u'_n)] du'_1 \cdots du'_n \\ &\approx 2^{i-1} \int_{u'_1 = \sqrt{\pi}/2}^{3\sqrt{\pi}/2} \cdots \int_{u'_{i-1} = \sqrt{\pi}/2}^{3\sqrt{\pi}/2} \int_{u'_i = -\sqrt{\pi}/2}^{\sqrt{\pi}/2} \cdots \int_{u'_n = -\sqrt{\pi}/2}^{\sqrt{\pi}/2} \left[\prod_{i=1}^n F(u'_i) \right] [1 - P_\alpha^i(u'_1, \dots, u'_n)] du'_1 \cdots du'_n, \end{aligned} \quad (\text{E6})$$

where $P_\alpha^i(u'_1, \dots, u'_n)$ is the success probability for the point $(u'_1, u'_2, \dots, u'_n)$ when $M_1, \dots, M_{i-2} \in \text{NPZ}, M_{i-1}, \dots, M_{n-1} \in \text{PZ}$,

$$\begin{aligned} P_\alpha^i(u'_1, \dots, u'_n) &= \frac{1}{2^{n-1}} \prod_{k_1=2}^{i-1} \left[\text{erf} \left(\frac{5\sqrt{\pi}/2 - u'_1 - u'_{k_1}}{\tilde{\Delta}} \right) - \text{erf} \left(\frac{3\sqrt{\pi}/2 - u'_1 - u'_{k_1}}{\tilde{\Delta}} \right) \right] \\ &= \times \prod_{k_2=i}^n \left[\text{erf} \left(\frac{3\sqrt{\pi}/2 - u'_1 - u'_{k_2}}{\tilde{\Delta}} \right) - \text{erf} \left(\frac{\sqrt{\pi}/2 - u'_1 - u'_{k_2}}{\tilde{\Delta}} \right) \right]. \end{aligned} \quad (\text{E7})$$

There are C_n^{i-1} cases giving the same result as the case i , so we need to add a factor C_n^{i-1} in the expression of the failure probability.

The failure probability of case $\frac{n+3}{2}$ is given by

$$P_{f,n\text{-rep}}^{\frac{n+3}{2}} = \sum_{j=\frac{n+1}{2}}^n C_n^j P_F^j (1 - P_F)^{n-j}. \quad (\text{E8})$$

Finally, the total failure probability of the n -qubit GKP repetition code is summation of the failure probabilities of all $(n+3)/2$ cases

$$P_{f,n\text{-rep}} = P_{f,n\text{-rep}}^1 + C_n^1 P_{f,n\text{-rep}}^2 + \sum_{i=3}^{\frac{n+1}{2}} C_n^{i-1} P_{f,n\text{-rep}}^i + P_{f,n\text{-rep}}^{\frac{n+3}{2}}. \quad (\text{E9})$$

APPENDIX F: FAILURE PROBABILITY OF GKP REPETITION CODE WITHOUT GKP ERROR CORRECTION

To calculate the failure probability of the GKP repetition code without one round of GKP error correction, we only need to replace $\{u'_i\}$ with distribution $F(u'_1, \dots, u'_n)$ in Eq. (E9) by $\{u_i\}$ with distribution $f_q(u_1, \dots, u_n)$ given by Eq. (5), and replace P_F by $P_{\tilde{X}}$, where $\{u_i\}$ are displacement errors of n data qubits without GKP error correction. The result is then given by

$$\begin{aligned}
P'_{f,n\text{-rep}}(\Delta, \tilde{\Delta}) &= \int_{u_1=-\sqrt{\pi}/2}^{\sqrt{\pi}/2} \cdots \int_{u_n=-\sqrt{\pi}/2}^{\sqrt{\pi}/2} f_q(u_1, \dots, u_n) [1 - P_{\alpha}^1(u_1, \dots, u_n)] du_1 du_n \\
&+ \sum_{m=1}^{\frac{n-1}{2}} C_n^m 2^m \int_{u_1=\sqrt{\pi}/2}^{3\sqrt{\pi}/2} \cdots \int_{u_m=\sqrt{\pi}/2}^{3\sqrt{\pi}/2} \int_{u_{m+1}=-\sqrt{\pi}/2}^{\sqrt{\pi}/2} \cdots \int_{u_n=-\sqrt{\pi}/2}^{\sqrt{\pi}/2} f_q(u_1, \dots, u_n) [1 - P_{\alpha}^{m+1}(u_1, \dots, u_n)] du_1 \cdots du_n \\
&+ \sum_{i=\frac{n+1}{2}}^n C_n^i P_{\tilde{X}}^i (1 - P_{\tilde{X}})^{n-i}.
\end{aligned} \tag{F1}$$

-
- [1] P. W. Shor, *Phys. Rev. A* **52**, R2493 (1995).
- [2] D. Gottesman, *Stabilizer Codes and Quantum Error Correction* (California Institute of Technology, Pasadena, CA, 1997).
- [3] B. M. Terhal, *Rev. Mod. Phys.* **87**, 307 (2015).
- [4] C. Weedbrook, S. Pirandola, R. García-Patrón, N. J. Cerf, T. C. Ralph, J. H. Shapiro, and S. Lloyd, *Rev. Mod. Phys.* **84**, 621 (2012).
- [5] S. L. Braunstein and P. van Loock, *Rev. Mod. Phys.* **77**, 513 (2005).
- [6] V. V. Albert, K. Noh, K. Duivenvoorden, D. J. Young, R. T. Brierley, P. Reinhold, C. Vuillot, L. Li, C. Shen, S. M. Girvin *et al.*, *Phys. Rev. A* **97**, 032346 (2018).
- [7] W. Cai, Y. Ma, W. Wang, C.-L. Zou, and L. Sun, *Fundamental Research* **1**, 50 (2021).
- [8] D. Gottesman, A. Kitaev, and J. Preskill, *Phys. Rev. A* **64**, 012310 (2001).
- [9] A. L. Grimsmo and S. Puri, *PRX Quantum* **2**, 020101 (2021).
- [10] P. T. Cochrane, G. J. Milburn, and W. J. Munro, *Phys. Rev. A* **59**, 2631 (1999).
- [11] T. C. Ralph, A. Gilchrist, G. J. Milburn, W. J. Munro, and S. Glancy, *Phys. Rev. A* **68**, 042319 (2003).
- [12] M. H. Michael, M. Silveri, R. T. Brierley, V. V. Albert, J. Salmilehto, L. Jiang, and S. M. Girvin, *Phys. Rev. X* **6**, 031006 (2016).
- [13] L. Hu, Y. Ma, W. Cai, X. Mu, Y. Xu, W. Wang, Y. Wu, H. Wang, Y. Song, C.-L. Zou *et al.*, *Nat. Phys.* **15**, 503 (2019).
- [14] Z. Ni, S. Li, X. Deng, Y. Cai, L. Zhang, W. Wang, Z.-B. Yang, H. Yu, F. Yan, S. Liu *et al.*, *Nature (London)* **616**, 56 (2023).
- [15] A. L. Grimsmo, J. Combes, and B. Q. Baragiola, *Phys. Rev. X* **10**, 011058 (2020).
- [16] S. Endo, Y. Suzuki, K. Tsubouchi, R. Asaoka, K. Yamamoto, Y. Matsuzaki, and Y. Tokunaga, *arXiv:2211.06164*.
- [17] K. Noh, V. V. Albert, and L. Jiang, *IEEE Trans. Inf. Theory* **65**, 2563 (2018).
- [18] C. Flühmann, T. L. Nguyen, M. Marinelli, V. Negnevitsky, K. Mehta, and J. Home, *Nature (London)* **566**, 513 (2019).
- [19] B. De Neeve, T.-L. Nguyen, T. Behrle, and J. P. Home, *Nat. Phys.* **18**, 296 (2022).
- [20] P. Campagne-Ibarcq, A. Eickbusch, S. Touzard, E. Zalys-Geller, N. E. Frattini, V. V. Sivak, P. Reinhold, S. Puri, S. Shankar, R. J. Schoelkopf *et al.*, *Nature (London)* **584**, 368 (2020).
- [21] V. Sivak, A. Eickbusch, B. Royer, S. Singh, I. Tsioutsios, S. Ganjam, A. Miano, B. Brock, A. Ding, L. Frunzio *et al.*, *Nature (London)* **616**, 50 (2023).
- [22] B. Q. Baragiola, G. Pantaleoni, R. N. Alexander, A. Karanjai, and N. C. Menicucci, *Phys. Rev. Lett.* **123**, 200502 (2019).
- [23] H. M. Vasconcelos, L. Sanz, and S. Glancy, *Opt. Lett.* **35**, 3261 (2010).
- [24] D. Su, C. R. Myers, and K. K. Sabapathy, *Phys. Rev. A* **100**, 052301 (2019).
- [25] M. Eaton, R. Nehra, and O. Pfister, *New J. Phys.* **21**, 113034 (2019).
- [26] J. Hastrup and U. L. Andersen, *Phys. Rev. Lett.* **128**, 170503 (2022).
- [27] R. Dahan, G. Baranes, A. Gorlach, R. Ruimy, N. Rivera, and I. Kammer, *Phys. Rev. X* **13**, 031001 (2023).
- [28] K. Fukui, A. Tomita, A. Okamoto, and K. Fujii, *Phys. Rev. X* **8**, 021054 (2018).
- [29] C. Vuillot, H. Asasi, Y. Wang, L. P. Pryadko, and B. M. Terhal, *Phys. Rev. A* **99**, 032344 (2019).
- [30] L. Hänggeli, M. Heinze, and R. König, *Phys. Rev. A* **102**, 052408 (2020).
- [31] K. Noh and C. Chamberland, *Phys. Rev. A* **101**, 012316 (2020).
- [32] J. E. Bourassa, R. N. Alexander, M. Vasmer, A. Patil, I. Tzitrin, T. Matsuura, D. Su, B. Q. Baragiola, S. Guha, G. Dauphinais *et al.*, *Quantum* **5**, 392 (2021).
- [33] K. Noh, C. Chamberland, and F. G. S. L. Brandão, *PRX Quantum* **3**, 010315 (2022).
- [34] H. Bombin and M. A. Martin-Delgado, *Phys. Rev. Lett.* **97**, 180501 (2006).
- [35] A. G. Fowler, *Phys. Rev. A* **83**, 042310 (2011).
- [36] J. Zhang, J. Zhao, Y.-C. Wu, and G.-P. Guo, *Phys. Rev. A* **104**, 062434 (2021).
- [37] J. P. Bonilla Ataides, D. K. Tuckett, S. D. Bartlett, S. T. Flammia, and B. J. Brown, *Nat. Commun.* **12**, 2172 (2021).
- [38] J. Zhang, Y.-C. Wu, and G.-P. Guo, *Phys. Rev. A* **107**, 062408 (2023).
- [39] O. Higgott, *ACM Trans. Quan. Comp.* **3**, 1 (2022).

- [40] M. P. Stafford and N. C. Menicucci, *Phys. Rev. A* **108**, 052428 (2023).
- [41] N. C. Menicucci, *Phys. Rev. Lett.* **112**, 120504 (2014).
- [42] I. Rojko, P. M. Röggl, M. Wägener, M. Fontboté-Schmidt, S. Welte, J. Home, and F. Reiter, [arXiv:2305.05262](https://arxiv.org/abs/2305.05262).
- [43] B. Royer, S. Singh, and S. M. Girvin, *Phys. Rev. Lett.* **125**, 260509 (2020).
- [44] A. J. Brady, A. Eickbusch, S. Singh, J. Wu, and Q. Zhuang, *Progress in Quantum Electronics* **93**, 100496 (2024).
- [45] K. Fukui, A. Tomita, and A. Okamoto, *Phys. Rev. Lett.* **119**, 180507 (2017).
- [46] Y. Xu, Y. Wang, E.-J. Kuo, and V. V. Albert, *PRX Quantum* **4**, 020342 (2023).
- [47] M. A. Nielsen and I. L. Chuang, *Quantum Computation and Quantum Information* (Cambridge University Press, Cambridge, England, 2010).
- [48] S. J. Devitt, W. J. Munro, and K. Nemoto, *Rep. Prog. Phys.* **76**, 076001 (2013).